



Lawrence Berkeley Laboratory

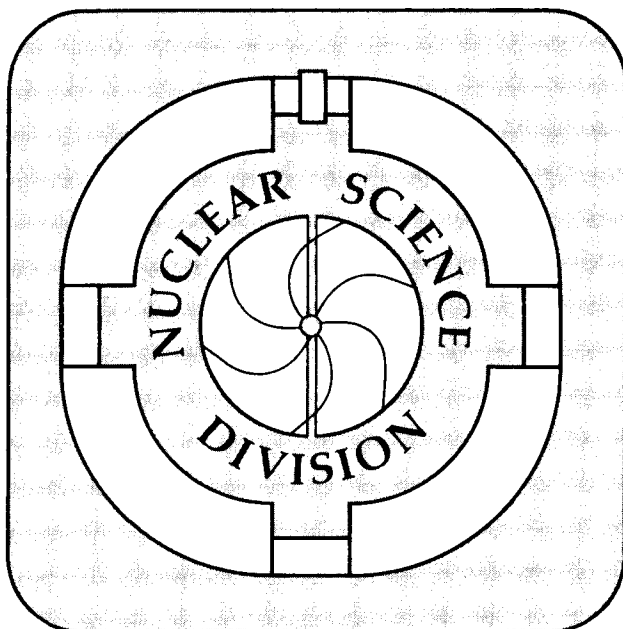
UNIVERSITY OF CALIFORNIA

Submitted to Nuclear Physics A

N-Body Collisions in High-Energy Nuclear Reactions

G. Batko, J. Randrup, and T. Vetter

July 1991



Prepared for the U.S. Department of Energy under Contract Number DE-AC03-76SF00098

1 LOAN COPY 1
1 Circulates 1
1 for 4 weeks 1 Bldg. 50 Library.
Copy 2

LBL-31031

DISCLAIMER

This document was prepared as an account of work sponsored by the United States Government. While this document is believed to contain correct information, neither the United States Government nor any agency thereof, nor the Regents of the University of California, nor any of their employees, makes any warranty, express or implied, or assumes any legal responsibility for the accuracy, completeness, or usefulness of any information, apparatus, product, or process disclosed, or represents that its use would not infringe privately owned rights. Reference herein to any specific commercial product, process, or service by its trade name, trademark, manufacturer, or otherwise, does not necessarily constitute or imply its endorsement, recommendation, or favoring by the United States Government or any agency thereof, or the Regents of the University of California. The views and opinions of authors expressed herein do not necessarily state or reflect those of the United States Government or any agency thereof or the Regents of the University of California.

N-Body Collisions in High-Energy Nuclear Reactions *

Gustavo Batko, Jørgen Randrup, and Thomas Vetter[†]
Nuclear Science Division, Lawrence Berkeley Laboratory
University of California, Berkeley, California 94720

July 18, 1991

ABSTRACT:

We study the effect of many-body collisions in simulations of nuclear dynamics. First, for elastic three-nucleon processes, the simplest pion-exchange diagrams are calculated and the ensuing scattering amplitude is used in a schematic calculation illustrating the evolution in momentum space. Then the collision integral in the *BUU* model is generalized to include many-body collisions. The number of baryons involved in a given collision is determined on the basis of the energy-dependent binary interaction range and their energy is shared microcanonically. This leads to a general treatment of *N*-body scattering (both elastic and inelastic) that can easily be incorporated into existing *BUU* codes. We study a variety of experimental observables, for the case of Ca+Ca at bombarding energies of 200-1000 MeV per nucleon, such as anisotropy, flow angle, sideways momentum, and backwards yield. The treatment is subsequently extended to include particle production and the production of kaons is especially considered. Overall, the results of the standard *BUU* model are affected relatively little by the incorporation of *N*-body collisions.

*This work was supported by the Director, Office of Energy Research, Office of High Energy and Nuclear Physics, Nuclear Physics Division of the U.S. Department of Energy under Contract No. DE-AC03-76SF00098.

[†]Supported by a grant from the Deutsche Akademische Austauschdienst (DAAD), Germany; now at the Institut für Theoretische Physik, Justus-Liebig-Universität, Gießen, Germany.

Contents

1	Introduction	1
2	Three-nucleon scattering	3
2.1	Pion-exchange model	3
2.2	Schematic studies	6
2.3	Conclusions from the schematic study	8
3	Extension of the BUU model	8
3.1	Specific model assumptions	9
3.1.1	Numerical solution of the BUU equation	10
3.1.2	Treatment of the collision term	11
3.2	Incorporation of N -body collisions	12
4	Dynamical simulations	14
4.1	Number of collisions	14
4.2	Collective flow	15
4.2.1	Thermalization and flow angles	15
4.2.2	Transverse momentum and stopping power	16
4.3	Backward scattering	17
4.4	Conclusions	17
5	Particle production	18
5.1	Microcanonical model for particle production	18
5.2	Elementary kaon cross section	19
5.3	Nucleus-nucleus collisions	21
6	Concluding remarks	22
A	Microcanonical selection of momenta	24
B	Effective production cross section	26
C	Cluster temperature	26

1 Introduction

Nuclear reactions at intermediate and high energies constitute a subject of central interest in modern nuclear physics. They offer the possibility for studying the behaviour of nuclear matter far from equilibrium, in highly excited and compressed systems.

Early theoretical descriptions of nucleus-nucleus collisions, such as those based on the fireball approximation [1, 2], succeeded in explaining most of the inclusive data but, as the experiments moved towards more exclusive measurements, dynamical models were needed in order to account for the observed data. The first fully microscopic description was provided by the cascade model [3]. Here each nucleus is represented by a collection of point nucleons and the reaction dynamics is determined by a sequence of binary collisions between hadrons. However, the absence of a mean field and Fermi momentum constituted a fundamental limitation. By combining the picture of individual hadronic collisions with a time-dependent effective one-body field, a more consistent description was obtained in terms of transport equations for the one-particle phase-space densities. This theory has been implemented under a variety of names, such as the Boltzmann-Uehling-Uhlenbeck (*BUU*) equation [4], the Vlasov-Uehling-Uhlenbeck equation [5], or the Landau-Vlasov equation [6]. It has formed the basis for a large number of dynamical simulations of high-energy nuclear collisions, for the purpose of extracting experimental information about the underlying nuclear dynamics and, especially, about the equation of state for nuclear matter [7, 8, 9, 10]. Examples are collective flow observables [11, 12], pion and photon production [13], dilepton emission [14, 15], and subthreshold production of heavy particles [9, 16].

Concurrent with this development, significant advances have also been made within the framework of quasi-classical many-body simulations, often referred to as molecular dynamics, and considerable success has been achieved with regard to reproducing a variety of experimental data; for a recent review, see ref. [17].

The formulation of the above mentioned transport theories has been discussed extensively in recent reviews [13, 18, 19]. Due to the complex nature of the nuclear many-body problem, the derivation of kinetic equations suitable for practical purposes requires the use of truncation schemes and cutting rules, thus limiting the applicability to specific energy domains. In the low-energy regime ($E \approx 10$ MeV per nucleon), the nuclear mean field and the Coulomb forces determine to a large extent the dynamical evolution of the system, since the occurrence of collisions is strongly suppressed due to the Pauli exclusion principle. This justifies the utilization of pure mean-field approaches, like those based on the *TDHF* equation or the Vlasov equation, its semi-classical analogue. In the intermediate-energy domain ($E \approx 10$ - 100 MeV per nucleon), the increasing availability of the phase space diminishes the effect of the Pauli principle and collisions become important. In this case, the global dynamics can be described by a *BUU*-like equation with an appropriate interaction as input. At higher energies ($E \gtrsim 100$ MeV per nucleon), the dynamics is mainly dominated by the collisions. In addition, the system reaches densities that may considerably exceed normal nuclear density. This feature, and the fact that the Pauli principle plays only a minor role, suggest that many-body collisions may be important. However, in the

applications done so far the dynamical description has been exclusively restricted to the level of two-body collisions.

The importance of involving more than two particles in the basic collision process (hereafter referred to as N -body collisions) was considered more than two decades ago by Bezzerrides and Du Bois [20], who derived corrections beyond two-body scattering processes to the Boltzmann equation. The first attempt to include N -body scattering processes in a dynamical simulation of a nucleus-nucleus collision was performed by Kodama *et al.* [21] by means of introducing a cluster approach to the cascade model. More recently, Bonasera and Gulminelli included three-body collisions in a simulation based on a transport equation [22]. Both calculations clearly showed that the contributions of non-binary processes are far from being negligible, especially in the high-energy domain, which suggests that the associated observables may be affected. However, due to the complicated phase-space evolution in a nucleus-nucleus collision, the magnitude of the effect is very difficult to estimate a priori.

From the kinematical point of view, N -body scattering processes contribute towards populating regions of the phase space that are less accessible through pure two-body processes. This feature might be relevant for the experimentally observed emission of high-momentum protons in the backward direction. In addition to the dynamical modifications of the nuclear phase space, an important probe of the occurrence of many-body collisions is the production of particles at energies below the free nucleon-nucleon threshold. In the picture of binary collisions the necessary energy is provided by the Fermi momentum. Additionally, subsequent binary collisions may eventually populate extreme regions of the phase space leading to highly energetic collisions. The inclusion of N -body collisions would provide an extra production mechanism, since more energy is available in the interaction of several nucleons.

Our main purpose is to study the effects of N -body collisions on observable quantities that are usually employed in the analysis of nuclear reactions at high energies. We begin, in sect. 2, by invoking the pion-exchange model for elastic three-nucleon scattering. This simplest example of a many-body collision is employed in a schematic study of the evolution in momentum space, considering a spatially uniform system. The incorporation of the N -body collisions into an actual dynamical simulation is accomplished by extending the standard *BUU* model; this is discussed in sect. 3. The extended *BUU* model is then applied to Ca-Ca reactions, in sect. 4, and the effect on various global observables is analyzed. Subsequently, a simple and general model for treating particle production in N -body scattering processes is developed in sect. 5, and the subthreshold production of kaons is especially considered and analyzed. Our general conclusions are made in sect. 6. In appendix A we discuss an approximate method for picking the momenta associated with the final state of the particles involved in a N -body collision. The derivation of the effective particle production cross section is presented in the appendix B, and its thermal aspects are discussed in appendix C.

2 Three-nucleon scattering

In this section we consider elastic scattering of three free nucleons, the simplest instance of the N -body scattering processes addressed in the present study. Employing a simple pion-exchange model, we calculate an analytical expression for the differential cross section and use this result in an instructive schematic study of the evolution in momentum space.

2.1 Pion-exchange model

We have calculated the two-pion-exchange three-nucleon interaction, because of its longest range. Figure 1 shows the pion-exchange diagram considered. The blob in fig. 1 represents everything which can happen for pion-nucleon scattering. For our purposes we study the case where the intermediate particle is either a nucleon or a delta. The scattering matrix element for the diagram in fig. 1 is given by

$$\begin{aligned}
 S_{fi} = & (-i)^4 \int \int \int \int d^4 x_1 d^4 x_2 d^4 x'_2 d^4 x_3 \left(\frac{m^6}{E_1 E_2 E_3 E'_1 E'_2 E'_3} \right)^{1/2} \\
 & \times \frac{e^{ip'_1 x_1}}{(2\pi)^{3/2}} \bar{u}(p'_1) \Gamma u(p_1) \frac{e^{-ip_1 x_1}}{(2\pi)^{3/2}} \frac{i}{(2\pi)^4} \int \frac{d^4 q}{q^2 - m_\pi^2 + i\epsilon} e^{-iq(x_2 - x_1)} \\
 & \times \frac{e^{ip'_2 x'_2}}{(2\pi)^{3/2}} \bar{u}(p'_2) \Gamma K(x'_2 - x_2) \Gamma u(p_2) \frac{e^{-ip_2 x_2}}{(2\pi)^{3/2}} \\
 & \times \frac{i}{(2\pi)^4} \int \frac{d^4 q'}{q'^2 - m_\pi^2 + i\epsilon} e^{-iq'(x_3 - x'_2)} \frac{e^{ip'_3 x_3}}{(2\pi)^{3/2}} \bar{u}(p'_3) \Gamma u(p_3) \frac{e^{-ip_3 x_3}}{(2\pi)^{3/2}} .
 \end{aligned} \tag{1}$$

For the sake of clarity we have suppressed the isospin indices in this formula. The matrix Γ describes the coupling of the baryons to the pions and K is the propagator for the intermediate particle.

Since we want to use the above S -matrix element for the description of three-nucleon scattering in nuclear collisions we must prevent the intermediate nucleon from being on the mass shell (which would render the matrix element infinite). Physically, the intermediate nucleon can only be on shell if an infinite time elapses between the two pion exchanges. Clearly, in the nuclear medium this cannot occur, because the intermediate nucleon can only travel a finite time, proportional to the mean free path of the nucleon in the medium. To account approximately for this key feature, we replace the free mass m_N in the nucleon propagator by \tilde{m}_N given as

$$\tilde{m}_N = m_N + \frac{i}{2} \Gamma_N, \tag{2}$$

where the width Γ_N is inversely proportional to the mean free path λ_N , $\Gamma_N = \hbar c / \lambda_N$. The nucleon propagator K is then given by

$$K_N(x - y) = \frac{i}{(2\pi)^4} \int d^4 p \frac{p_\mu \gamma^\mu + m_N}{p^2 - \tilde{m}_N^2 + i\epsilon} e^{-ip(x-y)}. \tag{3}$$

For an intermediate Δ this problem does not occur since the Δ has a finite lifetime, with a measured width $\Gamma_\Delta = 115$ MeV. Therefore the Δ mass also acquires an imaginary part,

$$\tilde{m}_\Delta = m_\Delta + \frac{i}{2}\Gamma_\Delta, \quad (4)$$

and the Δ propagator is

$$K_\Delta(x-y) = \frac{i}{(2\pi)^4} \int d^4p \frac{p_\mu \gamma^\mu + m_\Delta}{p^2 - \tilde{m}_\Delta^2 + i\epsilon} \times \left[-g^{\mu\nu} + \frac{1}{3}\gamma^\mu \gamma^\nu - \frac{1}{3m_\Delta}(\gamma^\mu p^\nu - p^\mu \gamma^\nu) + \frac{2}{3m_\Delta^2} p^\mu p^\nu \right] e^{-ip(x-y)}. \quad (5)$$

The $NN\pi$ vertex is given by

$$\Gamma_{NN\pi} = ig_{NN\pi} \bar{u}(p') \gamma_5 u(p), \quad (6)$$

where the pseudoscalar coupling has been used for the interaction of the nucleons with the pions, while the $\Delta N\pi$ vertex can be expressed as

$$\Gamma_{N\Delta\pi} = i \frac{f_{N\Delta\pi}}{m_\pi} \bar{\Delta}_\mu(p') q^\mu u(p). \quad (7)$$

To account for the finite sizes of the baryons, form factors are used at all vertices,

$$F(q) = \frac{\lambda^2 - m_\pi^2}{\lambda^2 - q^2}, \quad (8)$$

which is the standard monopole form.

Integrating (1) yields the familiar momentum space representation of the S -matrix element,

$$S_{fi} = \left(\frac{m^6}{E_1 E_2 E_3 E'_1 E'_2 E'_3} \right)^{1/2} \frac{1}{(2\pi)^5} \delta^4(p_1 + p_2 + p_3 - p'_1 - p'_2 - p'_3) \times \bar{u}(p'_1) \Gamma u(p_1) \frac{1}{q^2 - m_\pi^2 + i\epsilon} \bar{u}(p'_2) \Gamma K(p) \Gamma u(p_2) \frac{1}{q'^2 - m_\pi^2 + i\epsilon} \bar{u}(p'_3) \Gamma u(p_3). \quad (9)$$

Here p is the momentum of the intermediate particle and $K(p)$ is the Fourier transform of the propagators (3) and (5). After averaging over the initial spin and isospin, and summing over the final spin and isospin by tracing out the matrices, we obtain the transition rate,

$$w_{fi}^N = \frac{9}{8} F g_{NN\pi}^8 \left(\frac{\lambda^2 - m_\pi^2}{\lambda^2 - q^2} \right)^4 \left(\frac{\lambda^2 - m_\pi^2}{\lambda^2 - q'^2} \right)^4 \times \left| \frac{1}{p^2 - \tilde{m}_N^2} \right|^2 \left(2p'_2 p p_2 p - p_2 p'_2 p^2 + m_N^2 \{ -2p'_2 p - 2p_2 p + p^2 + p_2 p'_2 + m_N^2 \} \right), \quad (10)$$

$$w_{fi}^\Delta = \frac{1}{4} F g_{NN\pi}^4 \frac{f_{\Delta N\pi}^4}{m_\pi^4} \left(\frac{\lambda^2 - m_\pi^2}{\lambda^2 - q^2} \right)^4 \left(\frac{\lambda^2 - m_\pi^2}{\lambda^2 - q'^2} \right)^4$$

$$\times \left| \frac{1}{p^2 - \tilde{m}_\Delta^2} \right|^2 \left(2B^2 p'_2 q' p_2 q' - B^2 p'_2 p_2 q'^2 + A^2 p'_2 p_2 \right. \\ \left. + 2m_N A B p'_2 q' + 2m_N A B p_2 q' + m_N^2 A^2 + m_N^2 B^2 q'^2 \right) , \quad (11)$$

with

$$F = \frac{1}{E_1 E_2 E_3 E'_1 E'_2 E'_3} \frac{1}{(2\pi)^{14}} \delta^4(p_1 + p_2 + p_3 - p'_1 - p'_2 - p'_3) \\ \times \frac{(-p'_1 p_1 + m_N^2)(-p'_3 p_3 + m_N^2)}{(q'^2 - m_\pi^2)^2 (q^2 - m_\pi^2)^2} , \\ A = m_N q' q + \frac{2}{3} m_N p q' - \frac{1}{3} m_N q'^2 - \frac{2m_N}{3m_\Delta^2} q' p p q - \frac{2}{3m_\Delta} (q' p)^2 \\ + \frac{1}{3m_\Delta} q' p q^2 - \frac{1}{3m_\Delta} p q q'^2 + m_\Delta q' q + \frac{2}{3} m_\Delta q' p - \frac{1}{3} m_\Delta q'^2 - \frac{2}{3m_\Delta} q' p p q , \\ B = q' q - \frac{2}{3} m_N^2 + \frac{1}{3} q'^2 - \frac{2}{3m_\Delta^2} q' p p q + \frac{m_N}{3m_\Delta} q' p \\ - \frac{m_N}{3m_\Delta} p q - \frac{2}{3} m_N m_\Delta - \frac{1}{3} q' p - \frac{1}{3} p q .$$

Here w_{fi}^N is the contribution to the transition rate from the diagram with the intermediate nucleon and w_{fi}^Δ is the term arising from the diagram with the intermediate Δ . Finally, to obtain the total transition rate for three nucleons with momenta p_1, p_2, p_3 to the final momenta p'_1, p'_2, p'_3 , we average over the the possibilities that either one of the nucleons 1,2, or 3 is the middle one in diagram in fig. 1. We also have to sum over all permutations of the final momenta.

Here we have ignored the interference terms which generally arise between diagrams differing only by a permutation of their final momenta. This simplifying approximation can be justified by the fact that these graphs have their maximal contributions in different kinematical regions so that the product of these terms can be neglected. We then obtain the result

$$w_{fi}^{total} = \frac{1}{3} (w(1) + w(2) + w(3)) , \quad (12)$$

where, for example,

$$w(1) = \sum_{\mathcal{P}} \left(w_{fi}^N(p_2, p_1, p_3, p'_i, p'_j, p'_k) + w_{fi}^\Delta(p_2, p_1, p_3, p'_i, p'_j, p'_k) \right) , \quad (13)$$

with $\sum_{\mathcal{P}}$ denotes the sum over all permutations of the indices i, j, k . Furthermore, $w(1)$ represents the contribution for which the nucleon with momentum p_1 is the middle one in fig. 1, and $w(2)$, and $w(3)$ are defined correspondingly.

2.2 Schematic studies

In order to gain some insight into the effect of the three-body scattering, we consider the evolution in momentum space for an idealized system of the type considered in ref. [23]: a periodic box filled in a spatially uniform manner with nucleons whose momenta initially occupy two disjoint Fermi spheres, the relative speed being chosen so as to correspond to the beam rapidity of the actual nucleus-nucleus collision of interest. In this schematic calculation, we ignore the Pauli blocking in the final state.

First we specify the ratio between two-body scattering and three-body scattering. According to this ratio we then pick either two or three nucleons randomly and let them collide. In case of two-body scattering the final momenta are chosen according to the differential cross-section taken from [7]. In case of three-body scattering the outgoing momenta are sampled according to the transition rate calculated in sect. 2.1. This is done as described below.

First the momenta are boosted into their *CM* frame, where they form a triangle in momentum space. Due to energy and momentum conservation, the outgoing momenta can be described in terms of five independent variables – the well-known Jacobi coordinates. These five variables have then to be chosen according to the transition rate (12). For the various parameters we use the following values, $g_{NN\pi} = 13.5$, $f_{N\Delta\pi} = 2.13$, and $\lambda_{NN\pi} = \lambda_{N\Delta\pi} = 1.2$ GeV. They were taken from Wellers [24], who obtained them by analyzing pion photoproduction from nucleons. Furthermore, the $\pi\Delta$ coupling constant is determined by the free decay width of the Δ , and for the width of the nucleon we use $\Gamma_N = \Gamma_\Delta = 115$ MeV.

Because the matrix element is strongly peaked, the von Neumann rejection method [25] is not suitable for this task. We therefore use a Metropolis algorithm [26]. However, because the transition rate depends also on the incoming momenta, we need to set up a sampling chain for each possible combination of the incoming momenta. This can be done with sufficient accuracy by discretizing the incoming channel. Thus, we consider the discrete values $|\mathbf{p}_i| = n_i p_0$ for the magnitudes of the initial momenta, where n_i is an integer and p_0 is a suitably chosen grid spacing. In that way each triangle is characterized by three integers n_1, n_2 , and n_3 , and for each of these triangles a separate Metropolis sampling is set up. The algorithm for picking the final momenta is designed so that the energy and momentum is exactly conserved in the collision. After the final momenta have been thus selected, they are boosted back into the original frame.

In order to compare the angular distribution of particles scattered according to the two-body scattering amplitude or the three-body transition rate, we have employed an initial distribution consisting of two Fermi spheres, each containing 4000 nucleons. The top portion of fig. 2 shows the angular distribution for the three beam energies 400, 800, and 2000 MeV per nucleon. The angle of the nucleons relative to the beam axis, as seen in the *CM* frame of the two Fermi spheres, is denoted by ϑ . If two nucleons scatter, they are selected from two different Fermi spheres, whereas in the case of three-body scattering one nucleon is chosen from the projectile sphere and the other two from the target sphere; hence the asymmetric distribution for $N = 3$. The differential cross section of two-body scattering exhibits an isotropic distribution at

400 MeV and becomes forward peaked at higher energies. The three-body transition rate shows a different behavior. Already at 400 MeV small transverse momentum transfers are favored, and at higher energies the angular distribution of three-body scattering also grows more forward peaked, but this effect is not as strong as for two-body scattering.

One might expect that the three-body scattering might increase the yield of nucleons into backward directions in nuclear collisions. This expectation is based on elementary kinematical considerations. For example, a nucleon in the projectile undergoing a three-body elastic collision with two nucleons in the target may be scattered into the backwards direction with as much as two thirds of the beam velocity.

To examine this feature in more detail, we have follow the time evolution of two Fermi spheres in momentum space. As a convenient time scale we have chosen the number of collisions per nucleon n_c , defined as

$$n_c = \frac{1}{A} (2N_2 + 3N_3) . \quad (14)$$

where A is the combined number of particles in the target and projectile, N_2 is the number of two-body collisions, N_3 is the number of three-body collisions. We record the fraction of nucleons that are scattered backwards into a cone with an opening angle of 48° in the laboratory frame. We also require these nucleons to have a momentum magnitude larger then the Fermi momentum. Based on a relativistic Maxwell-Boltzmann distribution, the equilibrium value for this fraction of nucleons can easily be computed, yielding 0.31% at 400 MeV, 0.30% at 800 MeV, and 0.24% at 2000 MeV.

The middle part of fig. 2 shows the calculated backward yield as a function of the elapsed time, expressed in term of collisions per nucleon, for the same three energies. One immediately notices that in the case of three-body scattering the backward yield rises steeply and then falls off towards the equilibrium value. This is true for all three beam energies, although at higher energies it takes the system substantially longer to reach the equilibrium value – about 12-15 collisions per nucleon in our calculations.

It is also remarkable that the maximum backward yield shifts with increasing beam energy towards the earlier stages in the process. At 400 MeV the maximum value is reached after about two collisions per nucleon, whereas for 2000 MeV beam energy the backward yield peaks at 1.5 collisions per nucleon. If we only consider two-body scattering, at 400 MeV the fraction of nucleons in the backward direction rises slowly and approaches the equilibrium value. At higher energies we also see the same “overshooting” effect as in the case of three-body scattering, however much smaller and also much later in time relative to the three-body case.

We have also made a calculation in which half of all collisions are three-body collisions and half are two-body collisions. In this case the maximum of the backward yield shifts to later stages in the collision, when compared with the case of full three-body scattering. Moreover, at 800 and 2000 MeV the maximum fraction of backward nucleons is slightly higher than for pure three-body scattering.

Finally, in order to gain information about the way the system approaches the

equilibrium, we have studied the evolution of the anisotropy Q is defined as

$$Q = \frac{1}{A} \sum_{\nu=1}^A \frac{p_{\parallel}^2(\nu) - \frac{1}{2}p_{\perp}^2(\nu)}{p^2(\nu)}, \quad (15)$$

where again A is the combined number of nucleons in the system, and $p_{\parallel}(\nu)$ and $p_{\perp}(\nu)$ is the parallel and perpendicular component of the momentum of particle ν , respectively. This definition implies that the initial anisotropy approaches one at high energy, whereas it vanishes for the equilibrium distribution which has spherical symmetry.

The lower portion of fig. 2 shows the anisotropy Q as a function of the number of collisions per nucleon. At all beam energies, the anisotropy falls off faster when we allow only three-body scattering, relative to the case of pure binary collisions. This is expected, since the three-body collisions give direct access to larger regions of phase space than can be reached by binary collisions. One also notices that the effect of three-body collisions on the anisotropy increases with increasing beam energy. At 2000 MeV the system with only three-body scattering has almost reached its equilibrium value. By contrast, the system in which only two-body scattering occurs only reaches an anisotropy of 0.4 even after 6 collisions per nucleon. Thus, the system is still far from its equilibrium state. This observation is also in accordance with what one would expect from the fraction of backward scattered particles in the middle portion of the figure.

2.3 Conclusions from the schematic study

The schematic study described above shows that the way in which the system approaches equilibrium depends significantly on the characteristics of the elementary scattering mechanism. When three-body scattering is included, the system reaches the equilibrium much faster than in the case of pure binary scattering, particularly at higher beam energies, as one can easily see in the lower-right panel of fig. 2, the plot of the anisotropy at 2000 MeV. Our calculations also show that the yield of nucleons in the backward direction shows a different behavior as a function of time (as measured by n_c) if three-body scattering is included: the number of backward nucleons rises steeply and then falls off towards its equilibrium value. However, we also see that after 3–4 collisions per nucleons this effect has almost vanished. This result suggests that in actual nuclear reactions it might be rather difficult to extract information of the effects of three-body scattering from the yield of backward emitted nucleons.

3 Extension of the BUU model

One of the most common methods used to describe the nucleus-nucleus collision dynamics is based on the Boltzmann-Uehling-Uhlenbeck transport equation, the *BUU* method. It includes the two essential ingredients that are necessary in order to account for the basic dynamical features: the time-dependent mean field and the nucleon-nucleon cross section. The central quantity of the model is the one-particle phase-

space density distribution, $f(\mathbf{r}, \mathbf{p}; t)$. The time evolution of $f(\mathbf{r}, \mathbf{p}; t)$ is governed by the transport equation

$$\left\{ \frac{\partial}{\partial t} + \frac{\mathbf{p}}{m} \cdot \nabla_{\mathbf{r}} - \nabla_{\mathbf{r}} U(\mathbf{r}; t) \cdot \nabla_{\mathbf{p}} \right\} f(\mathbf{r}, \mathbf{p}; t) = I_{coll}[f]. \quad (16)$$

The left-hand side is the collisionless Vlasov term describing the evolution of the phase-space density in the one-body field only, while the right-hand side is the collision integral representing the average rate of change of the phase-space density due to the occurrence of direct collisions between the constituent hadrons¹. In general, the mean-field as well as the collision term depends on the many-body correlations in the system. When only the one-particle distribution is followed, one is forced to assume that the particles are mutually independent, which amounts to making the standard *Stoßzahlansatz*, and the collision integral is then a functional of the single-particle phase-space density.

In the treatments developed so far, only two-body collisions have been considered and the collision term is then given by

$$I_{coll}[f_1] = \frac{1}{2} \int d\mathbf{p}_2 d\mathbf{p}'_1 d\mathbf{p}'_2 T(\mathbf{p}_1 \mathbf{p}_2; \mathbf{p}'_1 \mathbf{p}'_2) (\bar{f}_1 \bar{f}_2 f'_1 f'_2 - f_1 f_2 \bar{f}'_1 \bar{f}'_2), \quad (17)$$

where $f_i \equiv f(\mathbf{r}, \mathbf{p}_i; t)$ and $\bar{f} \equiv 1 - f$ denotes the blocking factor expressing the availability of a phase-space cell near the specified phase-space location. The collision integral has a transparent physical meaning. The first term represents the contribution for scattering into the phase-space element $(\mathbf{r}, \mathbf{p}_1)$ and is therefore called the gain term, while the second term accounts for scattering out of that phase-space element and is called the loss term. Both are proportional to the occupation probability of the initial state two-particle state and to the probability that the final two-particle state is not blocked due to the Pauli exclusion principle. The quantity $T(\mathbf{p}_1 \mathbf{p}_2; \mathbf{p}'_1 \mathbf{p}'_2)$ is the transition rate associated with the elementary two-body scattering process. Although formal consistency requires that the transition rate and the effective field be determined from the same nucleon-nucleon interaction, this is rather impractical and, consequently, more approximate treatments are called for.

3.1 Specific model assumptions

The temporal evolution of the one-body phase-space distribution depends upon the specific assumptions made on the basic input quantities. As we have mentioned above, present computational capabilities do not permit the implementation of a treatment in which the cross sections and the mean field are fully consistent. Therefore, for the time being, it is necessary to express the mean field in terms of some convenient parametrization and use the experimentally known free NN cross sections.

¹Efforts to extend the *BUU* description to incorporate the effects of the fluctuations inherent in the basic nucleon-nucleon collisions are presently underway, see in particular refs. [27, 28]

As is usually done, the functional dependence of the one-body field on the one-body density f is assumed to be given by the Skyrme parametrization,

$$U(\rho) = A \frac{\rho}{\rho_0} + B \left(\frac{\rho}{\rho_0} \right)^\sigma . \quad (18)$$

The coefficients $A < 0$ and $B > 0$ are fitted in order to reproduce nuclear ground-state properties. We have employed the power $\sigma = 4/3$ in the Skyrme energy functional (18), corresponding to a nuclear compressibility $K = 238$ MeV, while $A = -219.2$ MeV and $B = 165.2$ MeV. The power σ is related to the nuclear compressibility. The Skyrme parametrization does not account for the well-established momentum dependence of the single-particle potential and occasionally a momentum-dependent term is added. For simplicity, we will neglect momentum-dependent forces and consider only static interactions, *i.e.* we retain only the above one-body field (18) and the Coulomb interaction.

We have included the following types of hadrons in our present calculations: the nucleon $N(940)$ and the baryon resonances $\Delta(1232)$ and $N^*(1440)$, and π mesons. We keep track of the different hadron isospin states, and use isospin-dependent cross sections, except for the elastic channels, where the standard Cugnon parametrization is employed [3]. The baryons are propagated according to the effective one-body field given by eq. (18), whereas the pions are treated as free particles.

We have included the following collision processes in the simulation

$$\begin{aligned} B_1 B_2 &\rightarrow B_1 B_2 , \\ NN &\rightleftharpoons N\Delta , \\ NN &\rightleftharpoons NN^* , \\ \Delta &\rightleftharpoons N\pi , \\ N^* &\rightleftharpoons N\pi . \end{aligned} \quad (19)$$

The decay of the resonances is governed by an exponential decay law and is assumed to be isotropic in the rest frame of the resonance. The parametrization of the cross sections associated with the processes (19), as well as the widths and life times of the resonances have been adopted from the values used by Wolf *et al.* [14].

3.1.1 Numerical solution of the BUU equation

The numerical problem of solving the *BUU* equation efficiently has been extensively discussed in the literature [7, 13, 14]. In order to establish the framework for describing how many-particle collisions are incorporated, we first review the main elements of the numerical realization of the model for the standard case when only the two-body collision term is considered.

The *BUU* equation can be solved by discretizing the phase-space density distribution, $f(\mathbf{r}, \mathbf{p}; t)$. This is done considering \mathcal{N} parallel systems of $A_T + A_P$ pseudo-baryons (and a dynamically determined number of pseudo-mesons), A_T and A_P being the target and projectile mass numbers, respectively. The associated baryon phase-space density distribution $f^{(n)}(\mathbf{r}, \mathbf{p}; t)$ for a particular system n in the ensemble is

then represented as

$$f^{(n)}(\mathbf{r}, \mathbf{p}; t) = \sum_{i=1}^{A_T+A_P} \delta(\mathbf{r} - \mathbf{r}_i^{(n)}(t)) \delta(\mathbf{p} - \mathbf{p}_i^{(n)}(t)), \quad (20)$$

where $(\mathbf{r}_i^{(n)}, \mathbf{p}_i^{(n)})$ is the phase-space trajectory of the i^{th} pseudo-baryon in the n^{th} system. The one-body density distribution for the system is then obtained as the average of the individual distributions for the \mathcal{N} parallel systems considered, $f = \sum_n f^{(n)}/\mathcal{N}$. In this manner, the fluctuations exhibited by the individual systems are suppressed after each time interval δt and a single dynamical trajectory $f(\mathbf{r}, \mathbf{p}, t)$ results, representing the approximate solution to the *BUU* equation (16).

It is straightforward to verify that, in the absence of collisions, eq. (20) is a solution of the *BUU* equation provided that the trajectories \mathbf{r}_i and \mathbf{p}_i satisfy the following hamiltonian equations of motion

$$\frac{d\mathbf{p}_i}{dt} = -\nabla_{\mathbf{r}} U(\mathbf{r}_i), \quad \frac{d\mathbf{r}_i}{dt} = \frac{\mathbf{p}_i c^2}{E_i}. \quad (21)$$

Note that the relativistic velocity $\mathbf{p}c^2/E$ has been used instead of \mathbf{p}/m , in order to take approximate account of the relativistic kinematics.

We simulate the time evolution of the phase-space density distribution using a sample of $\mathcal{N} = 700$ parallel systems of pseudo-particles. The density is calculated considering a time interval $\delta t = 0.5$ fm/c after which the new positions and momenta of the pseudo-particles are computed according to the equations of motion (21). In order to reduce the numerical noise due to the finite size of the sample, we use a gaussian smearing procedure to achieve smooth densities and reliable Pauli-blocking factors, as described in ref. [13]. Furthermore, to speed up the computations, only a subset of the systems are employed for the calculation of the spatial density $\rho(\mathbf{r})$. Due to the gaussian smearing, a subset of 100 systems already provides a reliable estimation of the density. In addition, the Pauli-blocking factors $\bar{f}(\mathbf{r}, \mathbf{p})$ have been estimated in a similar way, but using a subset of only 30 systems. We found that an increase in these sample sizes does not yield a significant improvement in the accuracy of the calculation and, therefore, increases the computing time unnecessarily.

The initial phase-space distribution of the pseudo-particles is obtained by assigning random positions according to a Woods-Saxon density distribution. The momenta are chosen randomly within a Fermi sphere whose radius is estimated locally in the Thomas-Fermi approximation. Then a boost is performed to ensure that the total momentum vanish and the resulting individual momenta are Lorentz boosted to the appropriate initial velocity of the nucleus. The values of the parameters used in the initialization procedure have been taken from ref. [13]. They reproduce ground-state properties and general nuclear stability with good accuracy.

3.1.2 Treatment of the collision term

In the model, the scattering of two baryons, $B_1 B_2 \rightarrow B'_1 B'_2$, is treated as a stochastic process involving four points in phase space.

In order to simulate the collision integral we have followed the prescription presented in ref. [14]. According to this prescription, the two particles may interact at their point of closest approach, provided this distance, d_{12} , is less than a predefined value $d_{max} = \sqrt{\sigma_{max}/\pi}$, where $\sigma_{max} = 55$ mb is the maximum of the energy-dependent nucleon-nucleon cross section. In order to minimize the effect due to the non-invariance of this collision criterion, we have used the covariant form of d_{12} . Moreover, the point in time at which the collision takes place has also been estimated relativistically, according to the convention of ref. [21]. Whether the particles actually interact is then decided randomly according to the probability $\sigma_{B_1 B_2 \rightarrow B_1 B_2}(E_{12})/\sigma_{max}$. When different channels are available in the final state, the specific collision channel is selected randomly according to the appropriate branching ratio $\sigma_{B_1 B_2 \rightarrow B'_1 B'_2}(E_{12})/\sigma_{max}$. The tentative final momenta are also assigned at random according to the corresponding differential cross section. Finally, whether such a tentative collision is actually realized is determined statistically on the basis of the blocking factor $\bar{f}'_1 \bar{f}'_2$ associated with the final two-particle state.

We stress that, consistent with the picture of \mathcal{N} parallel systems, collisions occur only between pseudo-particles belonging to the same system.

3.2 Incorporation of N -body collisions

It has been shown [20, 19], that the scattering rates in a many-body system can be expanded in the number of interacting particles. Accordingly, the collision integral can be written as

$$I_{coll}[f] = I_{coll}^{(2)}[f] + I_{coll}^{(3)}[f] + I_{coll}^{(4)}[f] + \dots \quad (22)$$

Since an N -body scattering process relates N points of the phase space in the initial state with N points in the final state, the generalization of eq. (17) to the N -body case is straightforward,

$$I_{coll}^{(N)}[f_1] = \frac{1}{N!} \int d\mathbf{p}_2 \cdots d\mathbf{p}_N d\mathbf{p}'_1 \cdots d\mathbf{p}'_N T(\mathbf{p}_1 \cdots \mathbf{p}_N; \mathbf{p}'_1 \cdots \mathbf{p}'_N) \times \left(\prod_{i=1}^N f_i \bar{f}_i - \prod_{i=1}^N f_i \bar{f}'_i \right), \quad (23)$$

where $T(\mathbf{p}_1 \cdots \mathbf{p}_N; \mathbf{p}'_1 \cdots \mathbf{p}'_N)$ denotes the associated N -body transition rate. Eq. (23) constitutes an extension of the results of ref. [20] to fermionic systems.

Although the above derivation is rather intuitive, it should be noted that the formalism follows from quantum many-body theory [19]. Although less rigorous, our presentation has the advantage of being conceptually simple and thus well suited for illustrating the physical contents of the theory.

In order to incorporate N -body collisions into this type of treatment we divide the problem into two parts: 1) the characterization of the N -body clusters that interact, and 2) the result of such an N -body interaction. With regard to the first aspect, we rely on basic dynamical picture provided by the *BUU* simulation. Thus assume that two baryons, B_1 and B_2 , are about to interact, according to the standard *BUU*

model described above. They are referred to as the *primary* baryons in that particular collision. We then examine the environment of the two primary baryons in order to determine which other baryons are located nearby, using the respective energy-dependent interaction ranges. This procedure may identify a number of neighboring baryons, B_3, \dots, B_N , which are assumed to also take part in the particular collision. Specifically, any pseudo-baryon B_j that belongs to the same system and whose distance to either one of the primary baryons is less than $\sqrt{\sigma_{B_i B_j}^{total}(E_{ij})}/\pi$, for $i = 1, 2$, is considered to be a part of the interacting N -body cluster. This simple prescription provides a well-defined mean of classifying the collision events according to their cluster size N . If there are no neighbors, we retain the usual binary scattering situation, but otherwise the additional members of the cluster may exchange energy and momentum with each other as well as with the primary baryons. Inelastic processes may occur only between B_1 and B_2 , according to the prescription explained in the previous section. Therefore, the additional $N - 2$ baryons are assumed to keep their identity during the collision process. Finally, as indicated in eq. (23), the effect of the Pauli exclusion principle is taken into account by considering the blocking factors associated to each particle in the final state of the N -body cluster.

Clearly, the calculation of all the relevant differential cross sections represents a formidable task which is beyond the scope of our present investigation. Rather, we adopt a conceptually simple and very general model for the outcome of the various N -body scattering processes. Specifically, for any given final channel, we assume that the available energy is distributed among the final particles according to the appropriate microcanonical distribution. Thus, apart from the constraints imposed by the conservation of energy and momentum, the outcome is assumed to be entirely statistical and the associated probability density is given by

$$\frac{d^{3N}P(\mathbf{p}'_1, \mathbf{p}'_2, \dots, \mathbf{p}'_N)}{d\mathbf{p}'_1 d\mathbf{p}'_2 \dots d\mathbf{p}'_N} \sim \delta(E - \sum_{i=1}^N \frac{(\mathbf{p}'_i)^2}{2m_i}) \delta(\mathbf{P} - \sum_{i=1}^N \mathbf{p}'_i), \quad (24)$$

where $E = \sum_i p_i^2/2m_i$ and $\mathbf{P} = \sum_i \mathbf{p}_i$ are the initial energy and momentum of the N particles, respectively. This is presumably an extreme assumption that will tend to overestimate the amount of energy-momentum exchange occurring between the primary particles and those in the proximity. Therefore, this treatment should provide a useful upper bound on the effect of incorporating N -body collisions. In Appendix A we describe an efficient approximate method for picking the final momenta.

We stress the following features of the adopted treatment: 1) the identification of N -body collisions is based on the two-body collisions calculated in the standard *BUU* model, 2) the many-body scattering is not based on microscopic matrix elements but on the simple but general principle of equipartition (implying, for example, isotropic angular distributions), and 3) possible in-medium effects on the cross sections have not been taken into account. Therefore, the model is expected to represent an extreme picture that must be considered as merely a useful starting point for investigating the manner in which the incorporation of many-body interactions could affect the observables extracted from dynamical simulations of nucleus-nucleus collisions.

4 Dynamical simulations

The model described in the preceding has been employed for the reaction $^{40}\text{Ca}+^{40}\text{Ca}$ at bombarding energies of 200, 600, and 1000 MeV per nucleon. In addition, we have performed the analysis for several values of the impact parameter in order to cover the complete range of events, from central to peripheral ones. Furthermore, we have included N -body collision processes involving clusters consisting of up to 10 baryons. The dynamical quantities calculated have also been compared with the standard *BUU* simulation that includes only binary collisions.

4.1 Number of collisions

Before we estimate the effect of N -body collision processes on the global dynamical quantities, it is interesting to consider the number of collisions that actually occurs in the simulation. Figure 3 shows the number of N -body collisions occurring in the course of a central event ($b=0$) as a function of the bombarding energy. The curves represent interpolations based on the values obtained at the above mentioned energies. The model shows that a significant fraction of the collision processes involves more than two baryons, particularly at bombarding energies larger than 600 MeV per nucleon. The relative frequency of N -body collisions increases with bombarding energy, as expected since higher densities are reached. Our results are in agreement with the calculations done by Bonasera and Gulminelli[22] for three-body collisions.

In fig. 4 we display the time dependence of the collision rate. The dashed histograms show the collision rate when only binary process are taken into account, while the results corresponding to binary, ternary, and quaternary processes are shown by the solid line histograms in decreasing order, respectively. The calculations indicate that multiple collisions predominantly occur during the high-density stage of the reaction.

In addition, we note that the number of binary collision clusters is significantly reduced when the possibility of N -body scattering is included, because collisions that were formerly treated as binary may now be considered as N -body processes. However, the total number of collisions changes by less than 3%. This is not surprising, since the occurrence of N -body collisions is closely tied to the occurrence of collisions between the primary baryons, according to our specific prescription. (Of course, the introduction of N -body collisions does change the dynamical evolution somewhat, but this has little effect on the total number of collisions occurring during the reaction.)

The effect of the Pauli-blocking can be readily appreciated from fig. 5. Note the sensitive decrease of the effect of the Pauli-blocking when the energy increases. In addition, we observe that the curves associated to different cluster size N scale approximately as $1 - f^N$, where f can be interpreted as an average occupation probability.

It is important to note that the relative contributions of the different N -body processes may depend on the equation of state employed (or equivalently, on the power σ in eq. (18)). At the same bombarding energy, a stiff equation of state would reduce the number of many-body collisions since the maximum nuclear density

reached by the system during the compressed phase is lower than in the present case. Conversely, a soft equation of state would enhance the number of N -body collisions.

4.2 Collective flow

We now discuss a number of global observables that are commonly employed in the analysis of relativistic nuclear collision events.

4.2.1 Thermalization and flow angles

The kinetic flow tensor analysis was adopted for the analysis of nuclear reactions for the purpose of elucidating the collective (fluid-dynamic) behaviour. A major motivation was the hope that such exclusive variables may offer a chance to extract experimentally the nuclear equation of state [29].

The flow pattern can be analyzed by constructing the kinetic flow tensor [30],

$$F_{ij} = \sum_{\nu=1}^{A_T+A_P} \frac{p_i(\nu)p_j(\nu)}{2m(\nu)}, \quad (25)$$

where $m(\nu)$ is the mass of the particle ν and $p_i(\nu)$ are the components of the corresponding three momenta. The symmetric tensor F specifies an ellipsoid in momentum space. The radii of the ellipsoid are related to the eigenvalues f_1 , f_2 and f_3 obtained by diagonalizing F , while the associated eigenvectors \mathbf{e}_1 , \mathbf{e}_2 and \mathbf{e}_3 define the direction of the principal axis. Let us order the eigenvalues so that $f_1 > f_2 > f_3$. In this way \mathbf{e}_1 corresponds to the direction of maximum kinetic flow. The polar angle with respect to the beam direction is called the flow angle θ_F .

The shape of the global flow pattern can be conveniently characterized in terms of the anisotropy parameter

$$Q = \frac{f_1 - \frac{1}{2}(f_2 + f_3)}{f_1 + f_2 + f_3}. \quad (26)$$

It is important to note that this parameter constitutes a measure of the degree of relaxation of the system, since a completely equilibrated system has an isotropic momentum distribution: $f_1 = f_2 = f_3$ yielding $Q = 0$. Therefore, the smaller the value of Q , the more thermalized is the system.

In order to perform the flow analysis we have proceeded as follows. For each system in our sample, we have constructed and diagonalized the kinetic flow tensor associated with the momentum distribution of the baryons at the end of the reaction. The resulting values of θ_F and Q are then binned in order to generate the corresponding probability distributions. Before showing the results it is important to make the following remark. In an ideal calculation, the flow vector lies always in the plane defined by the direction of the impact parameter and the beam axis – the impact plane. In practice, however, the reaction plane (as defined by the flow direction) generally deviates from the impact plane, due to the numerical fluctuations as well as to the violation of the conservation of angular momentum in the simulation of the collision

term. Nevertheless, these spurious effects average out and the mean flow vector lies approximately in the impact plane. However, the tilting angle ϕ_F associated with a particular system can deviate significantly from the ensemble average value [31]. In order to illustrate the magnitude of this effect, the calculated probability distributions of the tilting angle ϕ_F are shown in fig. 6. At $b=1.5$ fm, the typical standard deviation is 50° and decreases to 35° at $b=3$ fm. Naturally, the largest deviations happen at a beam energy of 200 MeV per nucleon. It is important to keep this in mind when comparing the calculated flow angle θ_F with those obtained from experimental data.

Figure 7 shows the resulting probability distributions of flow angles θ_F obtained when only binary collisions are considered (upper figures) and with the inclusion of N -body collisions (lower figures), for $b=1.5$ fm at the various bombarding energies. At 200 MeV per nucleon, the two different sets of calculation display similar flow angle distributions. However, at higher energies the inclusion of multiparticle collisions slightly increases the occurrence of larger flow angles, as compared to those obtained considering pure binary collisions. This behaviour is consistent with the fact that N -body collisions have an isotropic angular distribution while, at high energies, the angular distribution associated to binary scattering is forward-backward peaked. The corresponding mean value of the flow angle, $\langle\theta_F\rangle$, is listed in table 1. Due to the decreasing number of participant nucleons, the averaged flow angle decreases at larger impact parameters. As a function of the beam energy, it drops off at both low and high energies. This behaviour has been noted previously by Das Gupta [12] in the collision Nb+Nb, also using a *BUU* calculation. We observe that the inclusion of N -body collisions increases the value of the flow angle, except at low energies where binary collisions generate the larger flow.

The probability distributions for the anisotropy parameter Q are displayed in fig. 8. There are only slight differences between the two distributions at low energy. At higher energies the calculation corresponding to N -body collisions shows somewhat smaller values of Q , as compared with the standard two-body calculation. The magnitude of this effect can be more clearly appreciated from the average anisotropy $\langle Q\rangle$, which is listed in table 2. The resulting values of $\langle Q\rangle$ indicate that thermalization is more easily achieved through N -body collisions.

4.2.2 Transverse momentum and stopping power

Another observable that is sensitive to the collective flow is the average transverse momentum in the reaction plane, considered as a function of the rapidity [29]. This quantity is displayed in fig. 9. The curves have been obtained by smoothing the corresponding histograms. It has been found by Blättel *et al.* [11], using a relativistic version of the *BUU* method, that the origin of the transverse momentum depends on the particular rapidity region considered. In comparison with the standard *BUU* calculation based on binary collisions (dashed lines), our results show that the inclusion of N -body collisions (solid line) increases by up to 30% the transverse momentum in the participant rapidity region at 1 GeV per nucleon. At lower bombarding energies, however, the differences appear to be very small, while the fluctuations associated with the numerical calculations are rather large.

In addition, in fig. 10 we show the resulting rapidity density distributions. At high energies, the inclusion of N -body collisions tends to produce an enhancement in the number of particles scattered into the midrapidity region, thus increasing the stopping power. However, the effect is less than 20%. As before, the numerical fluctuations are large and tend to obscure the tiny differences that may appear at low energies.

4.3 Backward scattering

As can be observed from the results of fig. 10, the N -body collisions have no noticeable effect at the edges of the rapidity spectra. This suggests that N -body collisions would not affect the backward particle spectra. Nevertheless, backward proton spectra have been reasonably described by means of multiparticle interactions in p -nucleus collisions [32]. It is important to mention, however, that the sampling statistics associated with this region of the phase space is very poor in the simulation. In fact, the results shown in the lower-right panel of fig. 2 indicate that the fraction of particles scattered backward after two collisions per nucleon (which corresponds approximately to the time-scale of a Ca-Ca reaction at 1000 MeV per nucleon) is 0.7% and 0.4%, for a 50% mixture of two-body and three-body collisions and pure two-body collisions, respectively.

A possible explanation for the absence of an effect in the dynamical simulation may be the subsequent rescattering of the nucleons that have experienced N -body collisions. As we have found, N -body collisions occur predominantly during the compressed phase of the reaction while the expansion phase is dominated by binary interactions. Therefore, the backward yield arising from N -body collisions could disappear due to the rescattering taking place during the expansion of the system. This effect was already noted in connection with the schematic study made in sect. 2, although evolving on a slower time scale. In the realistic simulation, however, dynamical effects may alter the time scale and lead to a faster equilibration in phase space. Furthermore, we have employed an isotropic angular distribution for the outcome of the N -body collisions which certainly reduces the backward yield.

4.4 Conclusions

The analysis of the various observables has shown that N -body collisions have little influence on the collective flow and that, consequently, the global dynamics is adequately described in terms of binary correlations only.

We again stress that our model constitutes a first approximation. The quantum-mechanical N -body scattering amplitudes differs from the microcanonical approximation that we have employed here. As we indeed found using the one-pion exchange model, the amplitude for three-body scattering leads to an anisotropic distribution. In addition, it is not clear whether the standard Skyrme parametrization of the effective field, eq. (18), which is based on a two-body interaction, is adequate for describing a simulation that includes N -body interactions.

With the exception of the study performed by Bonasera and Gulminelli[22], the role of the nuclear equation of state in connection with N -body collisions has not

been investigated before. It is reasonable to expect that a change in the nuclear compressibility would be reflected in a change of the ratio of N -body to two-body collisions. However, due to the smallness of the effect of N -body collisions on the global observables, it seems unlikely that the use of a different equation of state could significantly change our present conclusions.

5 Particle production

For practical reasons, the available data related to particle production is limited to processes containing at most two particles in the initial state. The description of particle production processes involving more than two initial particles must therefore rely on theoretical assumptions. As a first step in this direction, we develop below a general model for incorporating particle production in N -body collision processes, based on a statistical picture.

5.1 Microcanonical model for particle production

In our present treatment we shall assume that when the two primary baryons B_1 and B_2 collide, the baryons B_3, B_4, \dots in their environment act as an energy reservoir similarly to the statistical picture adopted in the preceding section. Thus, the initial baryons are assumed to share their energy microcanonically, before the two primary baryons B_1 and B_2 produce a particle.

In the present exposition, we shall use non-relativistic kinematics which is simpler to treat. However, by employing suitable transformations, it is possible to extend the treatment to the relativistic regime as well. This aspect is further discussed in Appendix A.

For the development of this picture it is useful to define the following functional,

$$\mathcal{I}_{E,\mathbf{P}}^N[f] = \int d\mathbf{p}_1 \dots d\mathbf{p}_N f(\mathbf{p}_1, \dots, \mathbf{p}_N) \delta(\mathbf{P} - \sum_{i=1}^N \mathbf{p}_i) \delta(E - \sum_{i=1}^N \frac{p_i^2}{2m_i}). \quad (27)$$

Here E and \mathbf{P} are total kinetic energy and total linear momentum of the N baryons, respectively, while $f(\mathbf{p}_1, \dots, \mathbf{p}_N)$ is a function of the N baryon momenta. The microcanonical average of the function f is then given by $\langle f \rangle = \mathcal{I}[f]/\mathcal{I}[1]$. Here the denominator is recognized as the microcanonical momentum space integral and can be evaluated analytically [33],

$$\mathcal{I}_{E,\mathbf{P}}^N[1] = \frac{2\pi}{\Gamma(\frac{3}{2}N - \frac{3}{2})} \left(\frac{m_1 \dots m_N}{M_N} \right)^{\frac{3}{2}} \left[2\pi \left(E - \frac{P^2}{2M_N} \right) \right]^{\frac{3}{2}N - \frac{5}{2}}, \quad (28)$$

where $M_N = \sum_i m_i$ is the sum of the N individual baryon masses.

Let us now consider the production of a particle a , for example a kaon. The elementary production process is assumed to be of the form $B_1 B_2 \rightarrow a + X$ and the associated elementary cross section is given $\sigma_{B_1 B_2 \rightarrow a}(\epsilon_{12})$, where ϵ_{12} is the kinetic energy of the two initial baryons B_1 and B_2 in their CM system. However, in contrast to

the pure binary production mechanism, in an N -body collision the available energy ϵ_{12} is no longer well defined since the primary baryons, B_1 and B_2 , may exchange energy with the baryons in the environment. Therefore, the associated effective production cross section must be obtained by averaging the elementary cross section over all possible momentum configurations of the N -body system. Thus, since we assume that the total energy E is shared microcanonically between the emerging particles, we have for the effective cross section

$$\begin{aligned}\sigma_{B_1 B_2 \dots B_N \rightarrow a}(E) &= \mathcal{I}_{E, \mathbf{0}}^N[\sigma_{B_1 B_2 \rightarrow a}]/\mathcal{I}_{E, \mathbf{0}}^N[1] \\ &= \frac{1}{\mathcal{I}_{E, \mathbf{0}}^N[1]} \int d\mathbf{p}_1 \dots d\mathbf{p}_N \sigma_{B_1 B_2 \rightarrow a}(\epsilon_{12}) \delta(\sum_i \mathbf{p}_i) \delta(E - \sum_i p_i^2/2m_i).\end{aligned}\quad (29)$$

The integrand depends only on the relative energy of the two primary baryons, ϵ_{12} . Therefore, it is possible to carry out the integral over the momentum of the baryons in the environment, $\mathbf{p}_3, \dots, \mathbf{p}_N$, as well as over the total momentum of the two primary baryons, $\mathbf{P} = \mathbf{p}_1 + \mathbf{p}_2$, exploiting the above result for the microcanonical integral (28) (see Appendix A). The $3N$ -dimensional integral can thus be reduced to one dimension,

$$\begin{aligned}\sigma_{B_1 B_2 \dots B_N \rightarrow a}(E^*) &= \frac{\Gamma(\frac{3}{2}N - \frac{3}{2})}{\Gamma(\frac{3}{2}N - 3)\Gamma(\frac{3}{2})} (E^*)^{-\frac{3}{2}} \\ &\quad \times \int_{\epsilon_0}^{E^*} d\epsilon_{12} \sigma_{B_1 B_2 \rightarrow a}(\epsilon_{12}) \epsilon_{12}^{1/2} \left(1 - \frac{\epsilon_{12}}{E^*}\right)^{\frac{3}{2}N-4},\end{aligned}\quad (30)$$

where E^* is the total kinetic energy in the CM of the N -body cluster, and the lower limit of the integral, ϵ_0 , denotes the production threshold.

If the elementary cross section can be expressed in terms of a power series in ϵ_{12} ,

$$\sigma_{B_1 B_2 \rightarrow a}(\epsilon_{12}) = \sum_{k=0}^{k_{max}} a_k \epsilon_{12}^k, \quad (31)$$

the integral appearing in (30) can be evaluated by elementary means, and the effective cross section can be written as

$$\sigma_{B_1 B_2 \dots B_N \rightarrow a}(E^*) = \frac{\Gamma(\frac{3}{2}N - \frac{3}{2})}{\Gamma(\frac{3}{2}N - 3)\Gamma(\frac{3}{2})} \sum_{k=0}^{k_{max}} a_k B_x\left(\frac{3}{2}N - 3, k + \frac{3}{2}\right) (E^*)^k, \quad (32)$$

where B_x is the incomplete beta function and $x = 1 - \epsilon_0/E^*$. Note that the factor in front of the summation can be written in terms of the complete beta function as $1/B(\frac{3}{2}N - \frac{3}{2}, \frac{3}{2})$.

5.2 Elementary kaon cross section

The knowledge of the relevant particle production mechanisms at the elementary level, as well as their associated cross sections, is essential in a model calculation.

However, due to the lack of theoretical description of the particle production vertices, the elementary cross sections are often given as a parametrization of the available experimental data.

In our present study we are especially interested in the effect of N -body collisions on subthreshold kaon production and so we may employ the simple parametrization proposed by Schürmann and Zwermann [34],

$$\sigma_{NN \rightarrow K^+} = 800 \left[\frac{p_{max}}{(\text{GeV}/c)} \right]^4 \mu b, \quad (33)$$

where p_{max} is the maximum possible kaon momentum given by

$$p_{max}^2 = \frac{1}{4s} [s - (m_N + m_\Lambda + m_K)^2][s - (m_N + m_\Lambda - m_K)^2]. \quad (34)$$

Here \sqrt{s} is the invariant energy and m_N , m_Λ , and m_K are the masses of the nucleon, the Λ -particle, and the kaon, respectively. This parametrization arises from phase-space considerations near threshold and has been fitted to the limited data available for the inclusive cross section $pp \rightarrow K^+ + X$ [35]. Close to the threshold, eq. (33) has the same functional dependence that arises from the one-pion exchange model, but it grows very inaccurate for large values of p_{max} . We stress that so far no data are available in the vicinity of the threshold. In the earlier parametrization proposed by Randrup and Ko [36], the cross section is proportional to p_{max} , which gives a much better description at large p_{max} but probably overestimates the cross section at small p_{max} . The parametrization suggested recently by Wu and Ko [9], resulting from a calculation based in the one-pion exchange model, includes terms up to the fourth order in p_{max} and has a quartic behavior near threshold while resembling the linear parametrization at higher energies.

The contribution to the kaon cross section arising from the different baryonic channels are related to the NN channel as suggested in ref. [36],

$$\sigma_{B_1 B_2 \rightarrow K} \approx \begin{cases} \sigma_{NN \rightarrow K} & \text{for } NN \\ \frac{3}{4} \sigma_{NN \rightarrow K} & \text{for } N\Delta \\ \frac{1}{2} \sigma_{NN \rightarrow K} & \text{for } \Delta\Delta \end{cases} \quad (35)$$

where no distinction is made between N and N^* , except for the difference in mass.

In order to utilize any of the above described parametrizations in our model, we need to express them in the form of eq. (31). Since we are interested in the subthreshold regime, we expand p_{max}^2 in powers of ϵ_{12} around the threshold energy ϵ_0 . To order ϵ_{12}^2 , the result is

$$p_{max}^2 = \alpha(\epsilon_{12} - \epsilon_0)(\epsilon_{12} + \beta\epsilon_0), \quad (36)$$

with

$$\begin{aligned}
\epsilon_0 &= m_N + m_\Lambda + m_K - m_{B_1} - m_{B_2} , \\
\alpha &= 1 - \frac{3m_K(M_0 - m_K)}{M_0^2} , \\
\beta &= \frac{2m_K M_0(M_0 - m_K)}{\epsilon_0[M_0^2 - 3m_K(M_0 - m_K)]} - 1 , \\
M_0 &= m_N + m_\Lambda + m_K .
\end{aligned}
\tag{37}$$

The coefficients a_k appearing in eq. (29) can then be obtained by inserting eq. (36) into the desired parametrization of the elementary cross section. We have adopted the parametrization given in eq. (33), since we believe it represents a reasonable and simple description of K^+ -production in the relevant energy regime close to the threshold, although it is not entirely accurate.

The resulting N -body K^+ cross section, $\sigma_{B_1 B_2 \dots B_N \rightarrow K^+}$, as a function of the total kinetic energy of the N -body system, for different values of N , is shown in fig. 11 by the solid lines. In addition, we have also shown the effective N -body K^+ -cross section as resulting from the parametrization $\sigma_{NN \rightarrow K^+} = 0.25 \text{ mb/GeV} (\epsilon_{12} - \epsilon_0)$ (dashed lines), which gives a good fit to the experimental data but overestimates the expected cross section in the neighbourhood of the threshold. The behaviour of the cross section for different values of N reflects the energy balance imposed by the microcanonical approximation between the primary and the environment baryons. In fig. 12 we show the average relative kinetic energy of those pairs of primary baryons that produce a kaon, $\langle \epsilon_{12} \rangle$, as a function of the total kinetic energy in the collision cluster, E^* . Although the addition of more particles to the initial state increases the overall amount of kinetic energy available, the assumption of a statistical sharing of the energy gives $\langle \epsilon_{12} \rangle - \epsilon_0 \approx (E^* - \epsilon_0)/N$. In other words, on the average the available energy for particle production is equal to the available kinetic energy *per nucleon* in the incoming channel. It implies that, if the primary baryons do not have enough energy to produce a kaon the environment may provide it but, conversely, they may also absorb any energy excess carried by the primary baryons decreasing or even suppressing the production.

5.3 Nucleus-nucleus collisions

In addition to the details of the elementary cross section, the production of particles in a nucleus-nucleus model calculation depends on how many individual baryon-baryon collisions carrying enough energy occur in the simulation. Therefore, we first analyze the energy spectrum of the different clusters. The calculated spectra, corresponding to the simulation of the system $^{40}\text{Ca} + ^{40}\text{Ca}$ at various bombarding energies and impact parameters, are indicated in fig. 13 as a function of the kinetic energy in the center-of-mass of the cluster, E^* . We only show the parts of the spectra that are relevant for the production of heavy particles. The curves have been obtained by means of smoothing the resulting histograms. We observe that N -body processes (solid lines)

become dominant at energies above the kaon threshold, when compared with binary processes. Furthermore, the tail of the distributions extends to rather high kinetic energies, as the cluster size N increases. There is, however, a reduction of about a 50% in the number of two-body clusters with respect to those obtained in a pure binary simulation, which have been indicated by the dashed lines.

In order to explore the possibility that N -body collisions modify the yield of particles in a nucleus-nucleus collisions we have calculated the associated kaon multiplicities using the model developed in the preceding sections. Let us briefly recall the method [13]. In a *BUU*-type simulation the production of particles in the sub-threshold regime is assumed to be a perturbative process, *i.e.* it does not affect the global dynamical evolution. The total kaon multiplicity, $\nu_K(b)$, for a given impact parameter b is given by

$$\nu_K(b) = \frac{1}{\mathcal{N}} \sum_{\text{all collisions}} \frac{\sigma_{B_1 B_2 \dots B_N \rightarrow K}(E^*)}{\sigma_{B_1 B_2 \dots B_N}^{\text{total}}(E^*)}, \quad (38)$$

where the total cross section has been approximated by

$$\sigma_{B_1 B_2 \dots B_N}^{\text{total}}(E^*) \approx \sigma_{B_1 B_2}^{\text{total}}(\langle \epsilon_{12} \rangle). \quad (39)$$

The contribution to the K^+ multiplicity arising from the different cluster sizes N are shown in fig. 14, in the case of a central $^{40}\text{Ca}+^{40}\text{Ca}$ collision. Although N -body collisions are more frequent than two-body collisions and carry more energy, the strong reduction in the elementary cross section plays an important role in suppressing the production of particles for increasing N . Furthermore, the decrease in the contribution arising from binary collisions due to the inclusion of non-binary processes is compensated by the extra yield coming from collisions with $N \geq 3$. We found that the total K^+ multiplicity, as calculated with the extended method, differs from the standard two-body calculation by 17% and 8% at 600 and 1000 MeV per nucleon, respectively. Therefore, the net result is that the total yield remains essentially unchanged when N -body processes are included. This result is not surprising, in view of our assumption of energy sharing – the production yield then depends essentially on the available energy per nucleon. This feature is analyzed in more detail in Appendix C.

6 Concluding remarks

At the densities reached in nuclear collisions at high energies the standard assumption of isolated two-body scattering is not well justified. Therefore, we have developed a treatment that incorporates many-body scattering processes in a dynamical *BUU*-type simulation of a nucleus-nucleus collision.

We have first made a detailed study of the simplest case, namely elastic scattering of three nucleons. The corresponding differential distribution has been calculated on the basis of a simple pion-exchange graph, with an off-shell intermediate baryon between two sequential pion exchanges. As a function of the energy, the angular

distribution always presents an anisotropic pattern, in contrast to the two-body scattering which is isotropic up to energies of about 400 MeV per nucleon. At higher energies, the three-body scattering becomes more forward peaked, although the effect is smaller than what is observed in the two-body case.

For a spatially uniform system, we have studied the evolution in momentum space for initial distributions describing interstreaming gases corresponding to the kinematics of high-energy nuclear collisions. Particular attention has been paid to the yield in the backward direction, because of speculations that N -body scattering may lead to an enhancement. Using three-nucleon scattering in the idealized scenario, we have found that the backward region is indeed more favored, but only early on in the reaction; subsequent collisions drive the momentum distribution towards the equilibrium distribution, which is independent of the specific collision mechanisms employed. However, equilibrium is achieved much faster than in the case of pure two-body collisions, particularly at high energies.

The inclusion of N -body collisions in a realistic dynamical simulation has been based on a *BUU* transport equation with an extended collision integral, into which the non-binary scattering processes can be included rather naturally. We have examined the role of the baryons situated in the proximity of two primary collision partners. Using the energy-dependent interaction distance between two baryons, as obtained from their energy-dependent free scattering cross section, we have established a criterion for determining how many baryons in the environment may affect a given two-body collision, thus obtaining a means for classifying each collision event according to its cluster size N . Then, invoking the assumption of complete statistical sharing between the particles in a collision cluster, we have formulated a general treatment of the N -body scattering for any value of N . On this basis, we have examined the effect of N -body collisions for the collision of two calcium nuclei at a range of relativistic energies. Overall, there is little effect in the commonly employed global observables, such as the flow tensor and the transverse momentum distribution, even though about half the collision clusters contain more than two particles. It must be emphasized, however, that some observables that may be more strongly affected by the inclusion of N -body scattering (like the backward yield) have rather poor statistics in the simulation, which makes it difficult to reach more detailed conclusions.

We have given special consideration to the effect of the N -body scattering on the subthreshold production of particles, since one might expect that such processes would be enhanced because of the larger amount of energy present of a N -body cluster, relative to the ordinary binary situation. We generalized the statistical model to particle production, assuming that the additional particles in a given cluster share their energy statistically with the two primary particles responsible for the production. This leads to a relatively simple and general model, and we have applied it to kaon production in Ca-Ca collisions. Despite the fact that about half the kaons are produced from clusters with $N > 2$, the net effect is remarkably small. This can be qualitatively understood by realizing that the additional particles in a given cluster act as a reservoir that may not only contribute energy but also drain energy away from the producing particle pair. The determining feature is then the effective temperature of the clusters and this quantity is not very dependent on the cluster size

N , since all the clusters are drawn from the same system.

In conclusion, then, we find that the results of the standard *BUU* dynamical simulations are not appreciably affected by the incorporation of N -body collisions. This simplifying feature supports the *BUU* model as a quantitatively useful tool for nuclear reactions at relativistic energies. It should be emphasized, though, that our present studies are carried out with a number of simplifying assumptions, such as equipartition within a collision cluster, and that in-medium effects in the cross sections are absent. There is still a need for making more elaborate studies, in particular for calculating and employing the relevant N -body collision diagrams.

This work was supported by the Director, Office of Energy Research, Office of High Energy and Nuclear Physics, Nuclear Physics Division of the U.S. Department of Energy under Contract No. DE-AC03-76SF00098. We wish to acknowledge useful discussions with Ulrich Mosel, who stimulated us to consider this problem. One of us (T.V.) thanks the Deutsche Akademische Austauschdienst (DAAD) for a fellowship supporting his stay at LBL.

A Microcanonical selection of momenta

In our numerical simulations of N -body scattering it is necessary to pick the momenta of N particles according to the corresponding microcanonical distribution. When non-relativistic kinematics suffices, this task can be accomplished quickly and efficiently by a recently developed exact sampling method [37]. However, at the energies considered in the present study, where the kinetic energies are not negligible relative to the particle masses, relativistic kinematics must be used, and the sampling problem is then considerably harder to treat. We have therefore developed a simple approximate sampling method. It is based on the non-relativistic method, but the magnitudes of the sampled momenta are reduced so as to conform with the conservation of the relativistic four-momentum.

In the present context, we are faced with the task of reassigning relativistic momenta to the N particles in a given collision cluster. Let their initial momenta be $\tilde{\mathbf{p}}_i, i = 1, \dots, N$, let their masses be $m_i, i = 1, \dots, N$. The total four-momentum is then known, so that the total relativistic energy in the *CM* frame, $E_R = \sqrt{s}$, can be calculated.

Working in the *CM* frame, we first choose a set of tentative momenta $\mathbf{p}_i, i = 1, \dots, N$ according to the non-relativistic distribution, using the method in ref. [37]. These momenta then satisfy the energy constraint

$$\sum_{i=1}^N \frac{\mathbf{p}_i^2}{2m_i} = \sum_{i=1}^N \frac{\tilde{\mathbf{p}}_i^2}{2m_i} = E_{NR}, \quad (\text{A.1})$$

where E_{NR} is the available non-relativistic energy. In order to obtain momenta that

satisfy the relativistic energy constraint,

$$\sum_{i=1}^N (\mathbf{p}_i^2 + m_i^2)^{1/2} = E_R, \quad (\text{A.2})$$

we then rescale the tentative momenta of the N particles,

$$\mathbf{p}_i \rightarrow \mathbf{p}_i' = \mathbf{p}_i \sqrt{1+x}. \quad (\text{A.3})$$

A first-order approximation for the shrinking parameter x can be obtained by inserting \mathbf{p}_i' into eq. (A.2) and expanding the square root,

$$E_R \approx \sum_{i=1}^N (\mathbf{p}_i^2 + m_i^2)^{1/2} \left(1 + \frac{\mathbf{p}_i^2}{2m_i} x\right), \quad (\text{A.4})$$

which implies that

$$x \approx [E_R - \sum_{i=1}^N (\mathbf{p}_i^2 + m_i^2)^{1/2}] / [\sum_{i=1}^N \frac{\mathbf{p}_i^2}{2m_i}]. \quad (\text{A.5})$$

With the knowledge of x , the \mathbf{p}_i' can be determined. The shrinking procedure can then be repeated until the desired accuracy in the energy conservation is achieved. We have found that the algorithm converges and the difference between E_R and $\sum_i (\mathbf{p}_i^2 + m_i^2)^{1/2}$ becomes negligible after only a few iterations. Finally, the momenta are Lorentz boosted appropriately, so that the specified total four-momentum is obtained.

It is clear that although this method yields momenta that satisfy the relativistic four-momentum constraint, the distribution generated is somewhat distorted – with respect to the magnitude distribution as well as the relative directions. In order to test performance of the method, we have considered the case of three-body scattering, because for three momenta the relativistic sampling can also be done directly by introducing the Jacobi variables. They enable us to write the phase-space distribution for the outgoing particles in terms of five independent variables, which can then be sampled by a von Neumann rejection method [25].

We have compared our “shrinking” method with the exact relativistic sampling for the following quantities,

$$\text{folding angle :} \quad \langle \theta \rangle = \left\langle \frac{2}{N(N-1)} \sum_{i < j}^N \frac{\mathbf{p}_i \cdot \mathbf{p}_j}{p_i p_j} \right\rangle, \quad (\text{A.6})$$

$$\text{momentum squared :} \quad \langle \mathbf{p}^2 \rangle = \left\langle \frac{1}{N} \sum_{i=1}^N \mathbf{p}_i^2 \right\rangle, \quad (\text{A.7})$$

and the associated variances. As a typical example, we have considered a sample of 30000 momentum triplets, each with a CM energy of 5.33 GeV, and required an energy tolerance of 0.1 MeV in the iteration. The results are summarized in table 3. Furthermore, fig. 15 shows the comparison of the momentum and energy distribution for the two methods. The method appears to provide a quite reasonable approximation – certainly adequate for our present exploratory purposes.

B Effective production cross section

We here simplify the expression (29) for the effective cross section for the production of a particle a when two primary baryons B_1 and B_2 collide in the presence of $N - 2$ additional baryons B_3, \dots, B_N .

Let us first define the total momentum of the two primary baryons, $\mathbf{P}_{12} = \mathbf{p}_1 + \mathbf{p}_2$, their relative velocity $\mathbf{v}_{12} = \mathbf{p}_1/m_1 + \mathbf{p}_2/m_2$, and their relative momentum $\mathbf{p}_{12} = \mu_{12} \mathbf{v}_{12}$, where μ_{12} is their reduced mass. Using non-relativistic kinematics, as is justified near threshold, the energy of the two baryons, can then be written as

$$E_{12} = E_1 + E_2 = \epsilon_{12} + \frac{P_{12}^2}{2M_{12}}, \quad (\text{B.1})$$

where $M_{12} = m_1 + m_2$. The first term, $\epsilon_{12} = p_{12}^2/2\mu_{12}$, is the intrinsic kinetic energy, while the second term represents the energy associated with the translational motion of the center of mass of the two-baryon system. The integral appearing in eq. (29) can be recast in terms of \mathbf{P}_{12} and \mathbf{p}_{12} ,

$$\begin{aligned} \sigma_{B_1 B_2 \dots B_N \rightarrow a}(E) &= \frac{1}{\mathcal{I}_{E, \mathbf{P}}^N(1)} \int d\mathbf{p}_{12} \sigma_{B_1 B_2 \rightarrow a}(\epsilon_{12}) \\ &\times \left\{ \int d\mathbf{P}_{12} d\mathbf{p}_3 \dots d\mathbf{p}_N \delta \left(\mathbf{p}_{12} - \mathbf{P}_{12} - \sum_{i=3}^N \mathbf{p}_i \right) \right. \\ &\times \left. \delta \left(E - \frac{p_{12}^2}{2\mu_{12}} - \frac{P_{12}^2}{2M_{12}} - \sum_{i=3}^N \frac{p_i^2}{2m_i} \right) \right\}. \end{aligned} \quad (\text{B.2})$$

The integral between brackets is recognized as the momentum-space integral corresponding to $N-1$ particles with masses M_{12}, m_3, \dots, m_N and momenta $\mathbf{P}_{12}, \mathbf{p}_3, \dots, \mathbf{p}_N$, respectively. Replacing this integral by its explicit expression, eq.(28), and expressing the remaining integration in terms of ϵ_{12} , we arrive at

$$\begin{aligned} \sigma_{B_1 B_2 \dots B_N \rightarrow a}(E^*) &= \frac{\Gamma(\frac{3}{2}N - \frac{3}{2})}{\Gamma(\frac{3}{2}N - 3)\Gamma(\frac{3}{2})} (E^*)^{-\frac{3}{2}} \\ &\times \int d\epsilon_{12} \sigma_{B_1 B_2 \rightarrow a}(\epsilon_{12}) \epsilon_{12}^{1/2} \left(1 - \frac{\epsilon_{12}}{E^*} \right)^{\frac{3}{2}N-4}, \end{aligned} \quad (\text{B.3})$$

which is a relatively simple one-dimensional integral that can be tabulated as a function of E^* , once the elementary cross section $\sigma_{B_1 B_2 \rightarrow a}$ is given.

C Cluster temperature

Here we show that the baryons in the interacting cluster can be considered as a thermal reservoir.

It is possible to rewrite the above expression (B.3) for the effective production cross section in an instructive manner by noting that the power can be approximated

by an exponential $(1 - x)^p \approx \exp(px)$,

$$\sigma_{B_1 B_2 \dots B_N \rightarrow a}(E^*) \approx (2\pi\mu_{12}\tau)^{-\frac{3}{2}} \int d\mathbf{p}_{12} \sigma_{B_1 B_2 \rightarrow a}(\epsilon_{12}) e^{-p_{12}^2/2\mu_{12}\tau}. \quad (\text{C.1})$$

Here we have made the replacement $\Gamma(\frac{3}{2}N - \frac{3}{2})/\Gamma(\frac{3}{2} - 3) \approx \frac{3}{2}N - 4$, so that the temperature parameter is given by $\tau = E/(\frac{3}{2}N - 4)$. This approximation is not optimally accurate (particularly at low N), but serves to ensure that the result be normalized correctly, *i.e.* if the elementary cross section is constant, then the effective cross section must have the same value. The above result shows that the other baryons in the cluster act approximately as a standard thermal reservoir, with an effective temperature given by

$$\tau = \frac{E^*}{\frac{3}{2}N - 4}. \quad (\text{C.2})$$

The same feature can be found by observing that the probability for producing the given particle with a specified momentum \mathbf{p} and energy $\epsilon = p^2/2\mu$ is given by the size of the correspondingly constrained momentum-space integral $\mathcal{I}_{E^*-\epsilon, \mathbf{p}}^{N-1}[1]$ (see the general definition in eq. (27)), relative to the unconstrained integral $\mathcal{I}_{E^*, \mathbf{0}}^N[1]$, because of our assumption of energy equipartition. Using the same approximation as above, we then find the following differential particle production probability,

$$\frac{d^3P}{d\mathbf{p}} = \frac{\mathcal{I}_{E^*-\epsilon, \mathbf{p}}^{N-1}[1]}{\mathcal{I}_{E^*, \mathbf{0}}^N[1]} \approx (2\pi\mu\tau)^{-\frac{3}{2}} e^{-p^2/2\mu\tau}. \quad (\text{C.3})$$

We have seen from eq. (29) that the relative energy of the two primary baryons, ϵ_{12} , is governed by a beta distribution. Hence the first energy moment of the modulation factor in the integrand in eq. (B.3) is given by $\langle \epsilon_{12} \rangle \approx 1/(N - 1)$, whereas the above approximate expression would yield $\langle \epsilon_{12} \rangle \approx 1/(N - \frac{8}{3})$. Therefore, if one adjusts the temperature parameter in the above Boltzmann distribution (C.1) to be $\tau = E/(N - 1)$, then the first moment of the modulation function is reproduced correctly as well.

References

- [1] G.D. Westfall, J. Gosset, P.J. Johansen, A.M. Poskanzer, W.G. Meyer, H.H. Gutbrod, A. Sandoval, and R. Stock, *Phys. Rev. Lett.* 37 (1976) 1202.
- [2] S. Das Gupta and A.Z. Mekjian, *Phys. Rep.* 72 (1981) 131.
- [3] J. Cugnon, T. Mizutani, and J. Vandermeulen, *Nucl. Phys.* A352 (1981) 505.
- [4] G.F. Bertsch, H. Kruse, and S. Das Gupta, *Phys. Rev. C* 29 (1984) 673.
- [5] H. Kruse, B.V. Jacak and H. Stöcker, *Phys. Rev. Lett.* 54 (1985) 289.
- [6] C. Gregoire, B. Remaud, F. Sébille, L. Vinet, and Y. Raffray, *Nucl. Phys.* A465 (1987) 317.
- [7] G.F. Bertsch and S. Das Gupta, *Phys. Rep.* 160 (1988) 189.
- [8] W. Cassing, G. Batko, B. Blättel, V. Koch, A. Lang, U. Mosel, K. Niita, K. Weber, and Gy. Wolf, *Nucl. Phys. A* 519 (1990) 357c.
- [9] J.Q. Wu and C. M. Ko, *Nucl. Phys. A* 499 (1989) 810.
- [10] See "The Nuclear Equation of State", Part A, ed. W. Greiner and H. Stöcker, Plenum Press, 1989.
- [11] B. Blättel, V. Koch, A. Lang, K. Weber, W. Cassing, and U. Mosel, *Phys. Rev. C* 43 (1991) 2728.
- [12] S. Das Gupta, in: *Proc. Intern. Conf. of Nuclear Physics*, eds. B.K. Jain and B.C. Sinha (World Scientific, Singapore, 1985) p. 70.
- [13] W. Cassing, V. Metag, U. Mosel, and K. Niita, *Phys. Rep.* 188 (1990) 364.
- [14] Gy. Wolf, G. Batko, W. Cassing, U. Mosel, K. Niita, and M. Schäfer, *Nucl. Phys. A* 517 (1990) 615.
- [15] L. Xiong, Z.G. Wu, C.M. Ko, and J.Q. Wu, *Nucl. Phys. A* 512 (1990) 772.
- [16] W. Cassing, G. Batko, U. Mosel, K. Niita, O. Schult, and Gy. Wolf, *Phys. Lett. B* 238 (1990) 25; W. Cassing, G. Batko, T. Vetter, and Gy. Wolf, *Z. Phys. A.* (in press); G. Batko, W. Cassing, U. Mosel, K. Niita, and Gy. Wolf, *Phys. Lett. B* 256 (1991) 331.
- [17] J. Aichelin, *Phys. Reports* 202 (1991) 233.
- [18] W. Botermans and R. Malfliet, *Phys. Rep.* 198 (1990) 115.
- [19] P. Danielewicz, *Ann. Phys.* 197 (1990) 154
- [20] B. Bezzerides and D.F. DuBois, *Phys. Rev.* 168 (1968) 233.

- [21] T. Kodama, S.B. Duarte, K.C. Chung, and R.A.H.S. Nazareth, Phys. Rev. Lett. 49 (1982) 536.
- [22] A. Bonasera and F. Gulminelli, Phys. Lett. B259 (1991) 399.
- [23] J. Randrup, Nucl. Phys. A314 (1979) 429.
- [24] F. Wellers, Rapport Dhh-N/Saclay No. 2526 (1988).
- [25] S.E. Koonin, *Computational Physics* (Benjamin/Cummings, Menlo Park, 1986).
- [26] N. Metropolis, A. Rosenbluth, M. Rosenbluth, A. Teller and E. Teller, J. Chem. Phys. 21 (1953) 1087.
- [27] S. Ayik, and C. Gregoire, Phys. Lett. B212 (1988) 269; Nucl. Phys. A513 (1990) 187.
- [28] Ph. Chomaz, G.F. Burgio, and J. Randrup, Phys. Lett. 245B (1990) 340; G.F. Burgio, Ph. Chomaz, and J. Randrup, Nucl. Phys. A529 (1991) 157.
- [29] P. Danielewicz and G. Odyniec, Phys. Lett. B 157 (1985) 146.
- [30] M. Gyulassy, K.A. Frankel, and H. Stöcker, Phys. Lett. B 110 (1982) 185.
- [31] G.D. Westfall, C.A. Oglivie, D.A. Cebra, W.K. Wilson, A. Van der Holen, W. Bauer, J.S. Winfield, D. Krofcheck, J. Karn, S. Howden, T. Li, R. Lacey, K.Tyson, and M. Cronqvist, Nucl. Phys. A519 (1990) 141c.
- [32] P. Danielewicz, Phys. Rev. C42 (1990) 1564.
- [33] J.A. López and J. Randrup, Nucl. Phys. A503 (1989) 183.
- [34] B. Schürmann and W. Zwermann, Phys. Lett B183 (1987) 31.
- [35] V. Flaminio *et al.*, CERN- HERA report 84-01.
- [36] J. Randrup and C.M. Ko, Nucl. Phys. A343 (1980) 519; *ibid.* A411 (1983) 537.
- [37] J. Randrup, Comp. Phys. Comm. 59 (1990) 439.

E (A MeV)	$b=1.5$ fm		$b=3$ fm	
	Binary	N -body	Binary	N -body
200	14.23	12.11	7.14	6.32
400	14.64	16.66	7.90	7.89
600	13.62	16.25	7.35	8.00
1000	11.63	15.92	6.08	7.59

Table 1: Flow angle.

The average flow angle θ_F in Ca-Ca reactions at various beam energies E and impact parameters b , with either the standard *BUU* model in which only binary collisions are considered, or with our extension to N -body collisions.

E (A MeV)	$b=0$		$b=1.5$ fm		$b=3$ fm	
	Binary	N -body	Binary	N -body	Binary	N -body
200	0.195	0.196	0.294	0.301	0.461	0.465
400	0.184	0.166	0.294	0.279	0.521	0.505
600	0.188	0.158	0.318	0.256	0.554	0.521
1000	0.227	0.156	0.350	0.280	0.587	0.528

Table 2: Anisotropy.

The average anisotropy $\langle Q \rangle$ for Ca-Ca reactions, as in table 1.

Method	$\langle \vartheta \rangle$	$\sigma^2(\vartheta)$	$\langle \mathbf{p}^2 \rangle$	$\sigma^2(\mathbf{p}^2)$
Momentum shrinking:	-0.4362	0.2492	2.405	1.505
Exact relativistic:	-0.4298	0.2749	2.418	1.648

Table 3: Momentum shrinking method.

Comparison of our approximate sampling method with an exact relativistic sampling for a three-nucleon system with a CM energy of 5.33 GeV. The displayed quantities are: the average folding angle (A.6), its variance, the average momentum squared (A.7), and its variance, for a sample size of 30000 momentum triplets.

Figure 1: Pion-exchange diagram.

The pion-exchange diagram considered. Initially the three nucleons have the four-momenta p_1 , p_2 , p_3 , and the corresponding final values are p'_1 , p'_2 , p'_3 . The pion exchanged between nucleons 1 and 2 has the four-momentum q , and the one subsequently exchanged between between 2 and 3 has the four-momentum q' . The intermediate nucleon or delta has the four-momentum p .

Figure 2: Backwards scattering.

The three columns refer to beam energies of 400, 800, and 2000 MeV, respectively. The top row shows the angular distribution of the nucleons in the CM frame of two Fermi spheres for beam energies of 400, 800 and 2000 MeV. The quantity ϑ denotes the angle of the nucleons with the beam axis, in the CM frame of the two Fermi spheres. The solid line represents the distribution of the three-body scattering process, in which we choose one particle from the projectile sphere and two from the target sphere. The dashed line represents the case of binary scattering. Here we choose one particle from each of the two Fermi spheres. The differential cross section for two-body scattering was taken from [7].

The middle row shows the fraction of nucleons scattered into a cone with an opening angle of 48° in the backward direction, as seen in the lab frame, and with a momentum larger than the Fermi momentum. The solid line (100%) refers to the case when all the collisions involve three nucleons, while the dash-dotted line (50%) is obtained when half of the collisions are three-body collisions and half are two-body collisions. The dashed line (0%) again represents the case of pure binary scattering.

The bottom row shows the anisotropy Q as a function of the elapsed average number of collisions per nucleon. The line styles are defined as in the middle row.

Figure 3: Number of N -body collisions.

Beam energy dependence of the number of effective N -body collisions in the simulation of $^{40}\text{Ca}+^{40}\text{Ca}$ at $b = 0$. The smooth curves represent interpolations of the values calculated at beam energies of 200, 600 and 1000 MeV per nucleon.

Figure 4: N -body collision rate.

Rate of effective collisions as a function of the reaction time. The dashed curves correspond to a simulation including only binary collisions. The solid curves denote the contributions due to two-body (highest curve), three-body (middle curve) and four-body collisions (lowest curve).

Figure 5: Blocking.

Percentage of blocked N -body collisions as a function of the beam energy. The curves represent interpolations of calculated values at 200, 600 and 1000 A MeV.

Figure 6: Out-of-plane flow.

The probability distribution of the tilting angle, ϕ_F , for different energies and impact parameters. The impact plane corresponds to $\phi_F = 0$. Smooth curves have been generated from histograms with a bin size of 9° .

Figure 7: Flow angle.

Probability distribution of flow angles θ_F in $^{40}\text{Ca}+^{40}\text{Ca}$ for $b=1.5$ fm, at different bombarding energies.

Figure 8: Anisotropy:

Probability distribution of the anisotropy parameter Q in $^{40}\text{Ca}+^{40}\text{Ca}$ for $b=1.5$ fm, at different bombarding energies.

Figure 9: Transverse momentum.

Average transverse momentum per particle projected into the impact plane, for different bombarding energies and impact parameters. The abscissa is the rapidity y , divided by the midrapidity y_0 (equal to half the rapidity difference between the two Fermi spheres). The smooth curves have been obtained from histograms. The dashed lines correspond to the standard two-body calculation while the solid lines indicates the results obtained including N-body collisions.

Figure 10: Rapidity density.

Rapidity density of the baryons, $d\nu/dy$, as a function of the reduced rapidity y/y_0 , for different bombarding energies and impact parameters. The curves are marked as in fig. 9.

Figure 11: Kaon yield.

Elementary kaon yield as a function of the kinetic energy available in the N -body cluster, for various cluster sizes N . The experimental points have been taken from ref. [35].

Figure 12: Relative kinetic energy.

The average relative kinetic energy of those pairs of primary baryons that produce a kaon, as a function of the available kinetic energy in the N -body cluster in which they are produced.

Figure 13: Energy spectra of the collision clusters.

Energy spectra of the clusters, $d\nu_N/dE^*$, occurring in a Ca-Ca reaction at several impact parameters and bombarding energies. The numbers at the solid curves indicate the various cluster sizes N . For reference, the dashes curves show the results obtained with the standard *BUU* model where only pure two-body collisions are considered.

Figure 14: Kaon multiplicity.

The contribution to the K^+ multiplicity, ν_K , arising from N -body collisions of various cluster size N .

Figure 15: Microcanonical momentum distribution.

The momentum and energy spectra obtained with our approximate picking procedure (solid), as compared with the exact relativistic result (dashed) for three nucleons with a total energy of $\sqrt{s} = 5.33$ GeV.

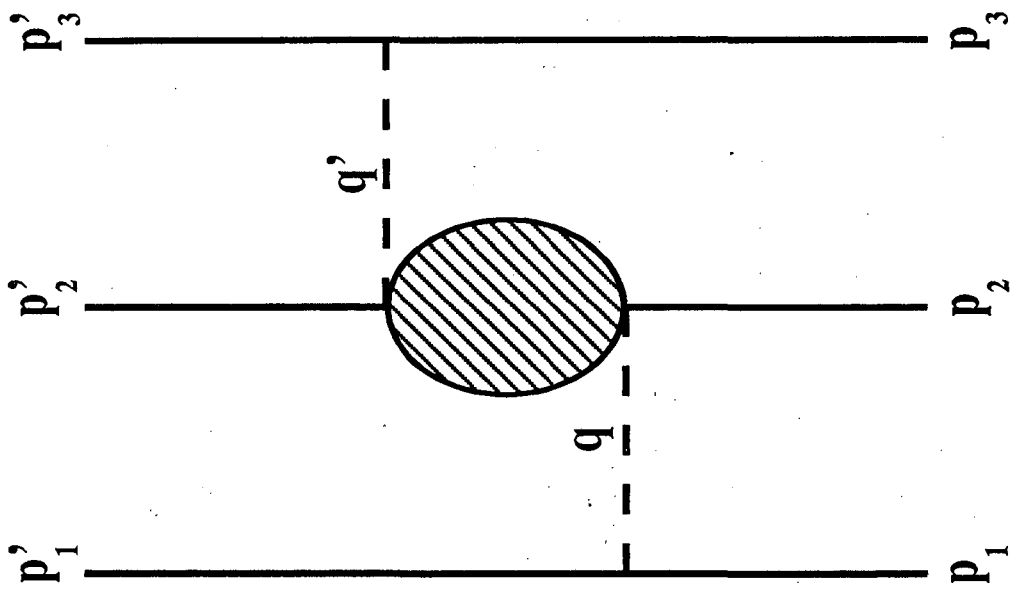
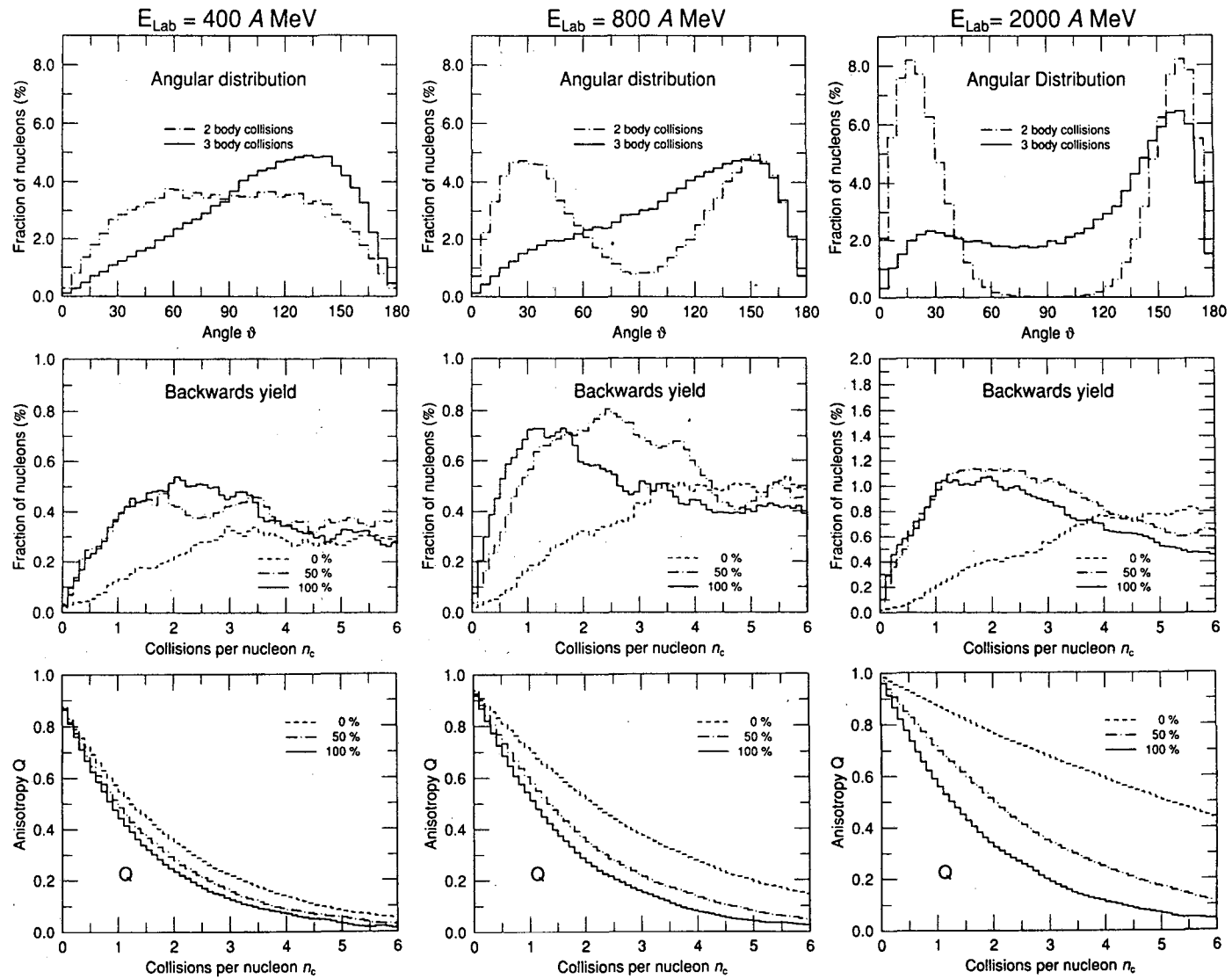


Figure 1



XBL 917-1460

Figure 2

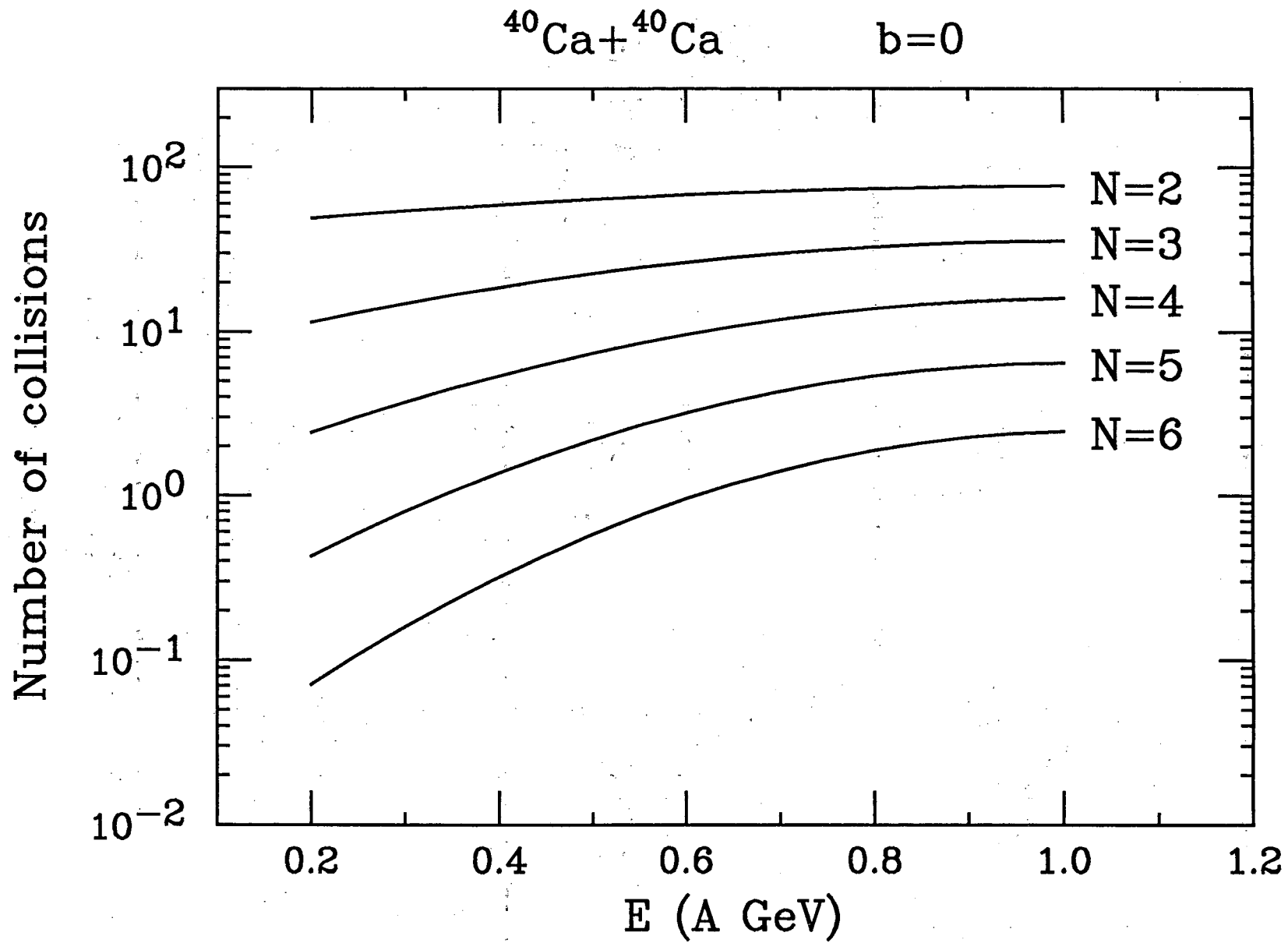


Figure 3

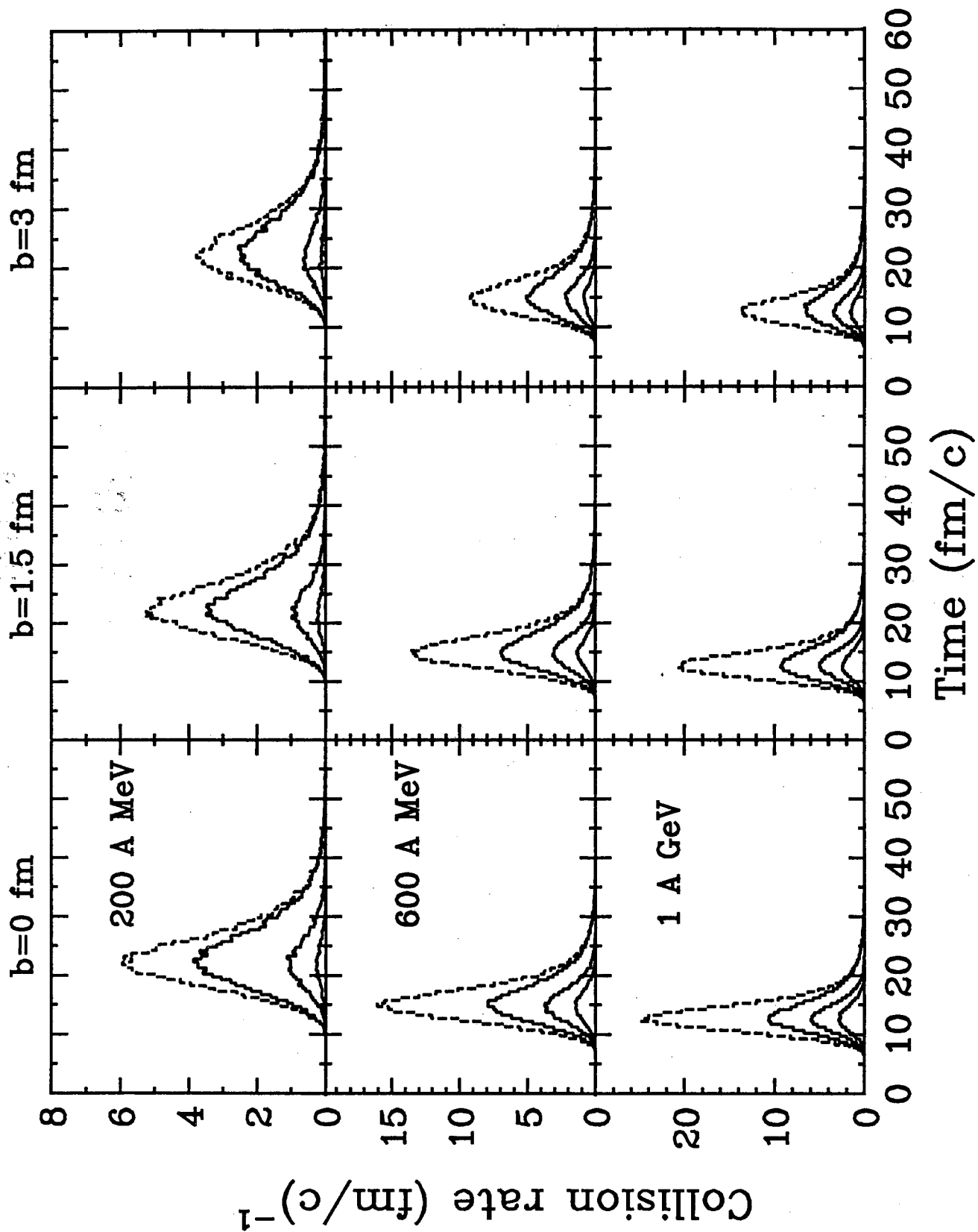


Figure 4

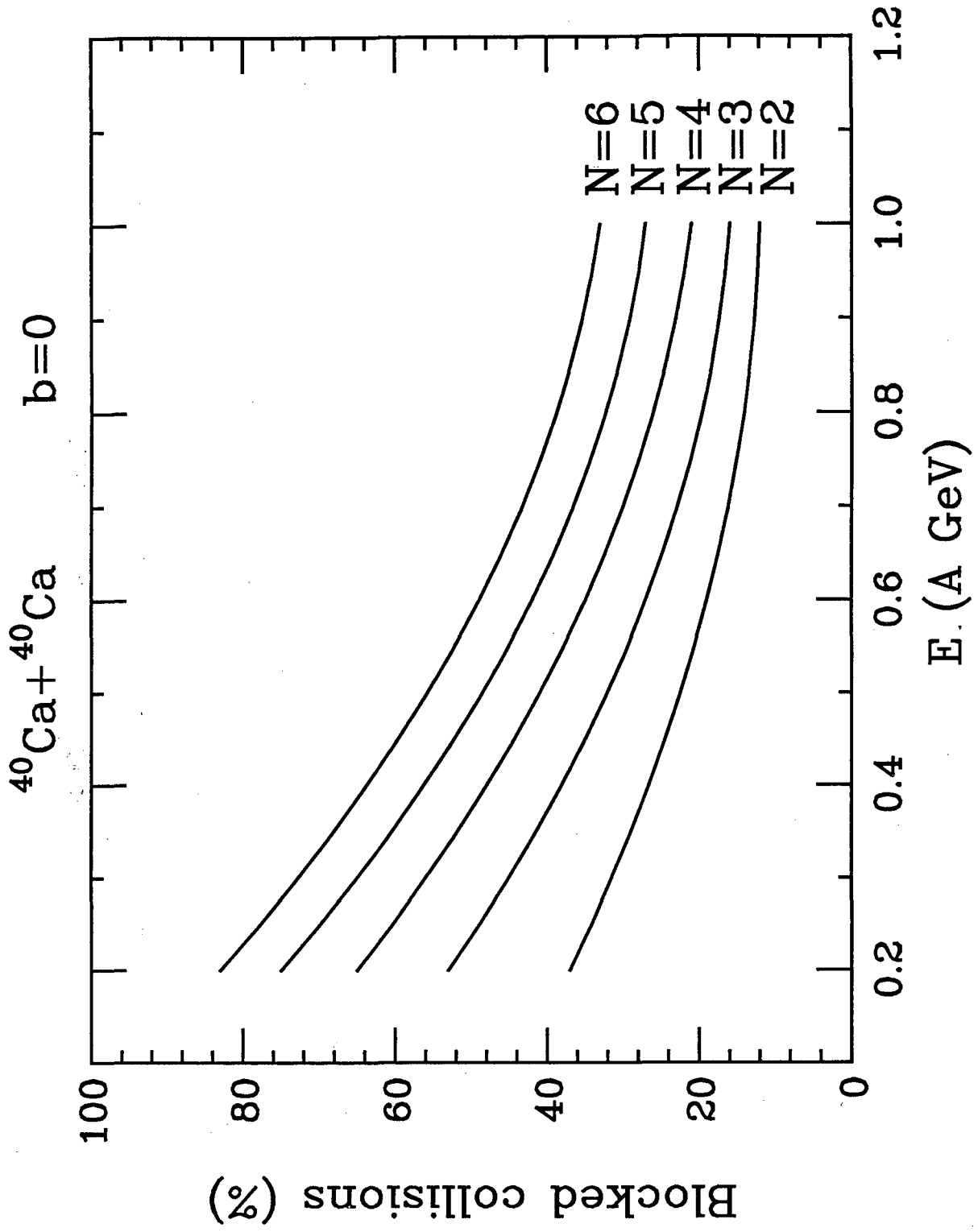


Figure 5

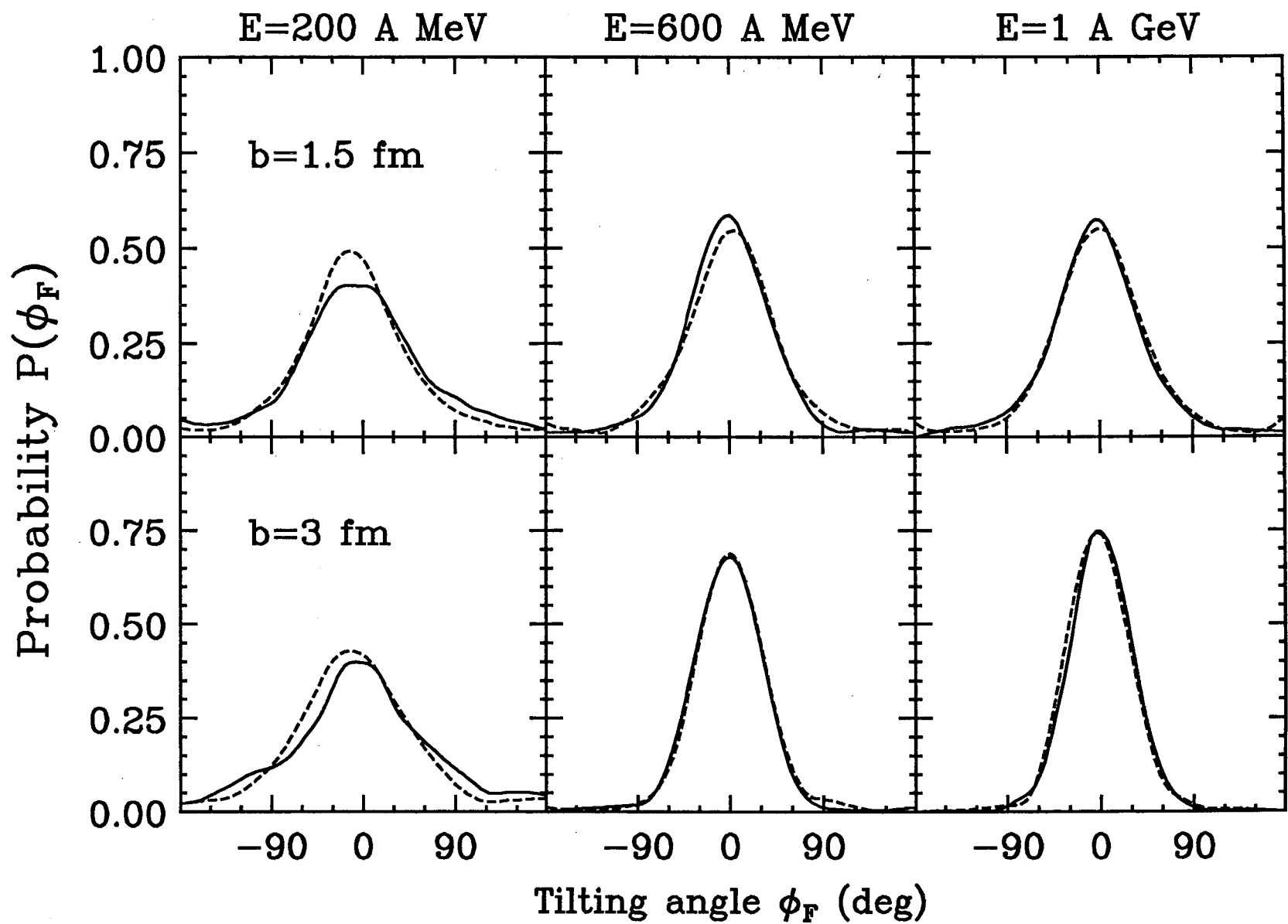


Figure 6

$^{40}\text{Ca} + ^{40}\text{Ca}$

$b = 1.5 \text{ fm}$

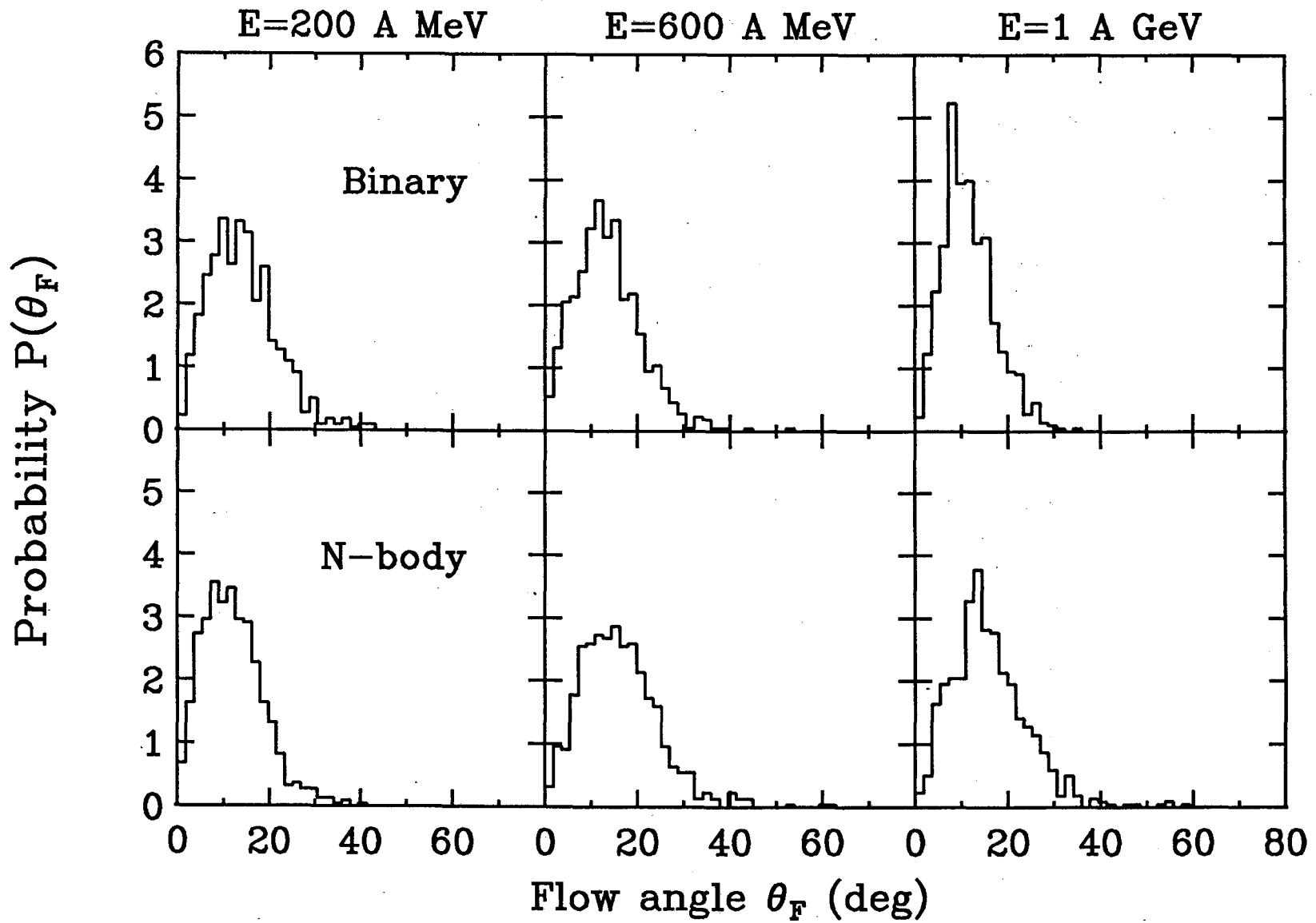


Figure 7

$^{40}\text{Ca} + ^{40}\text{Ca}$

$b = 1.5 \text{ fm}$

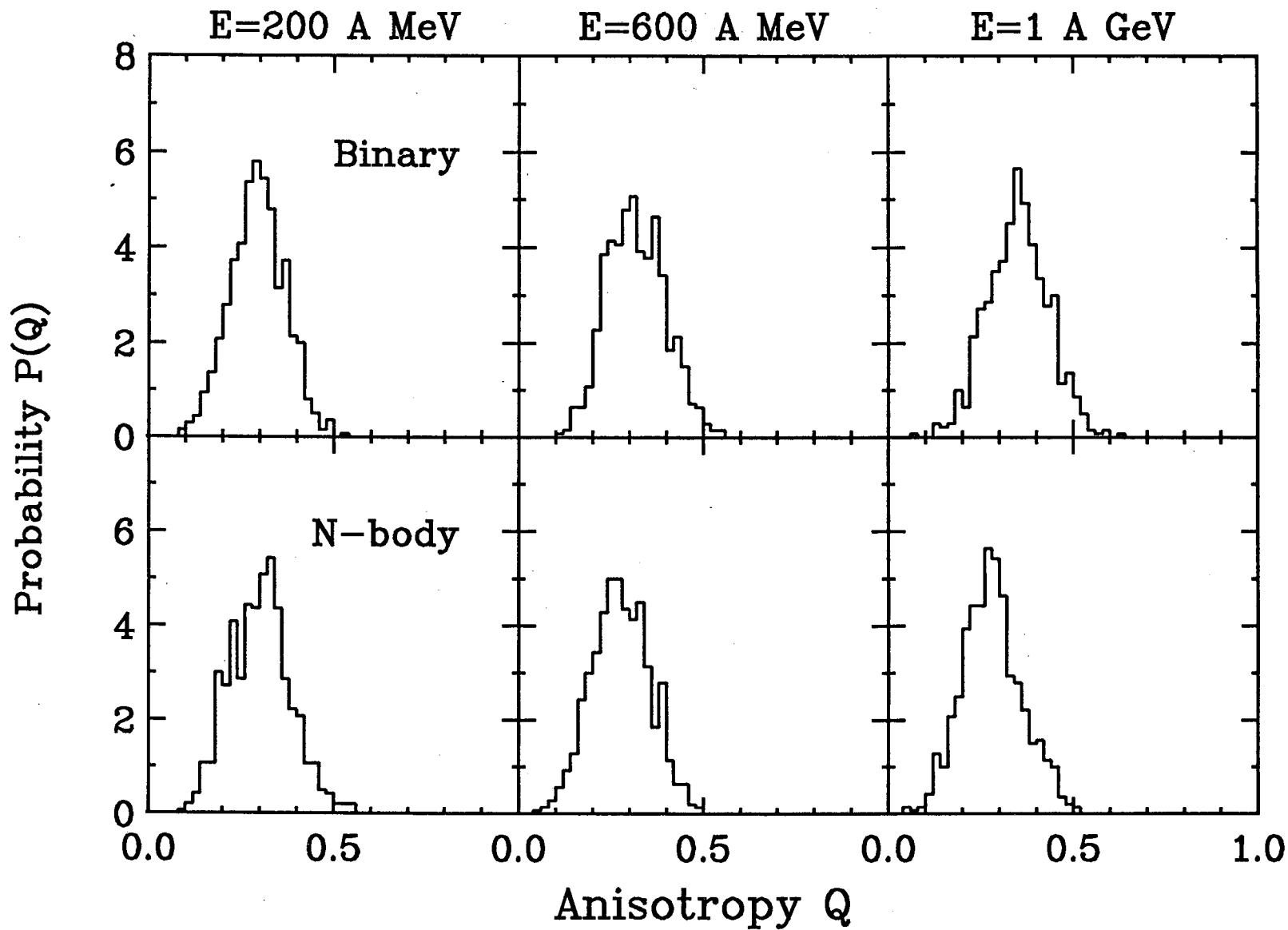


Figure 8

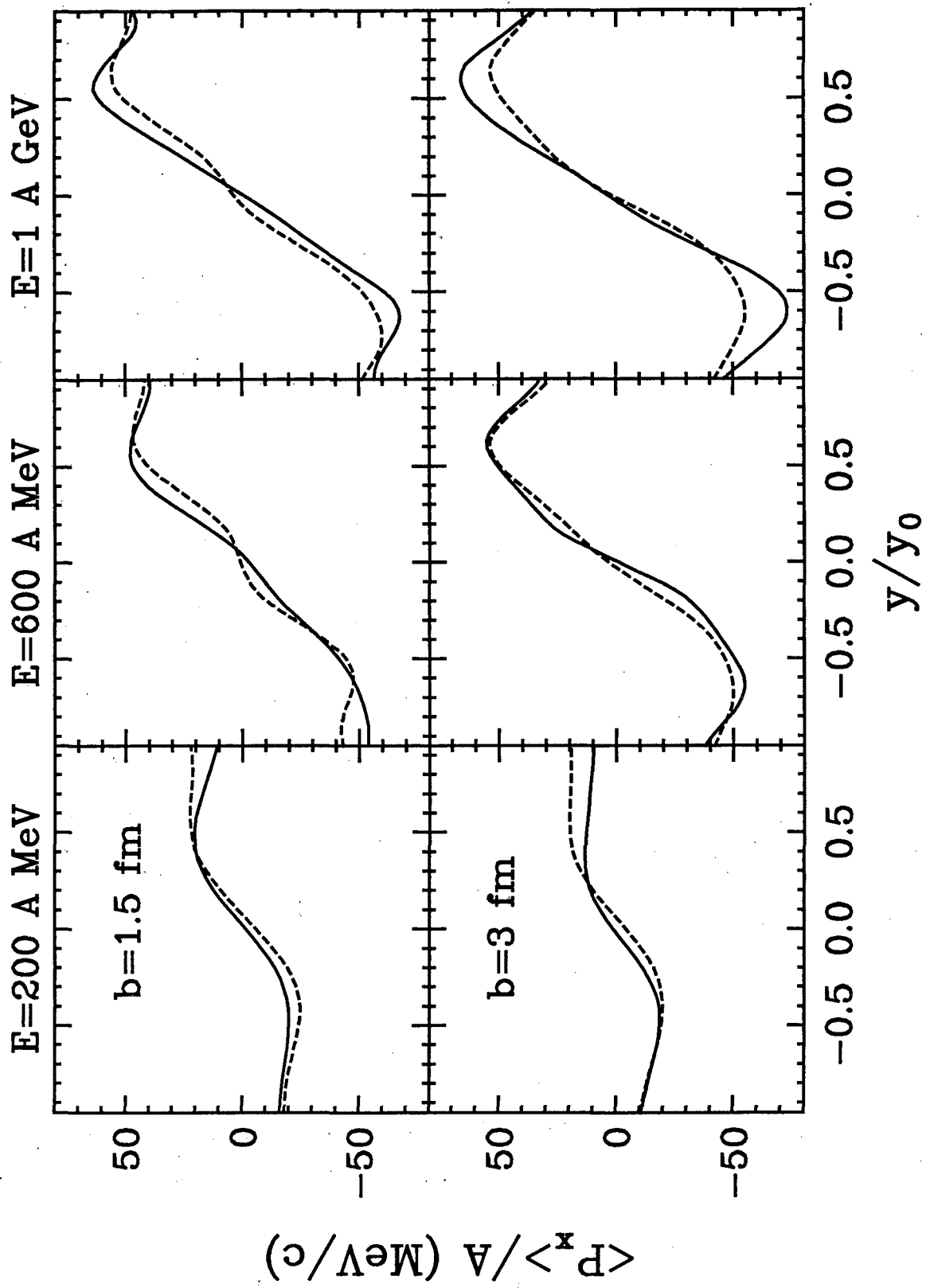


Figure 9

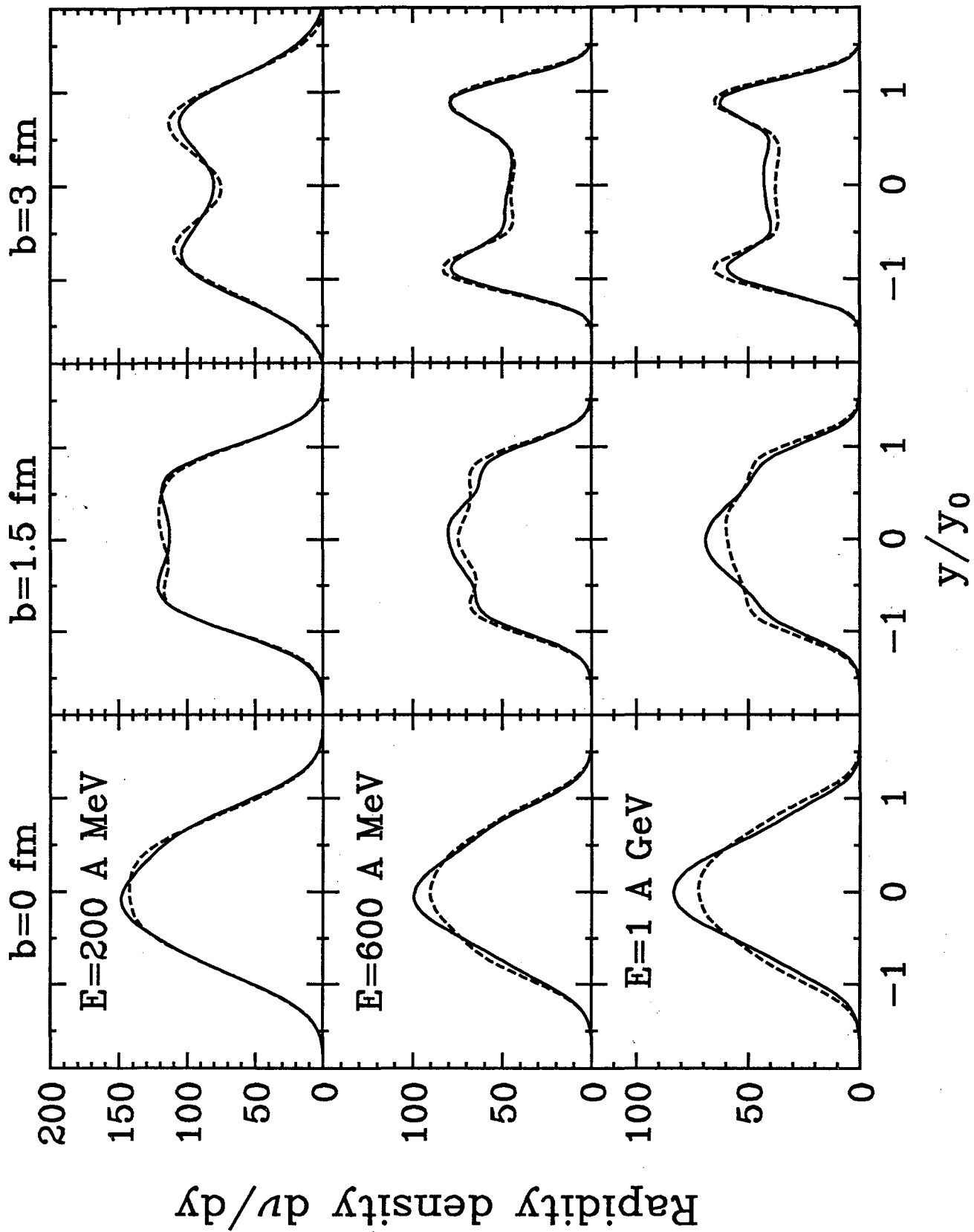


Figure 10

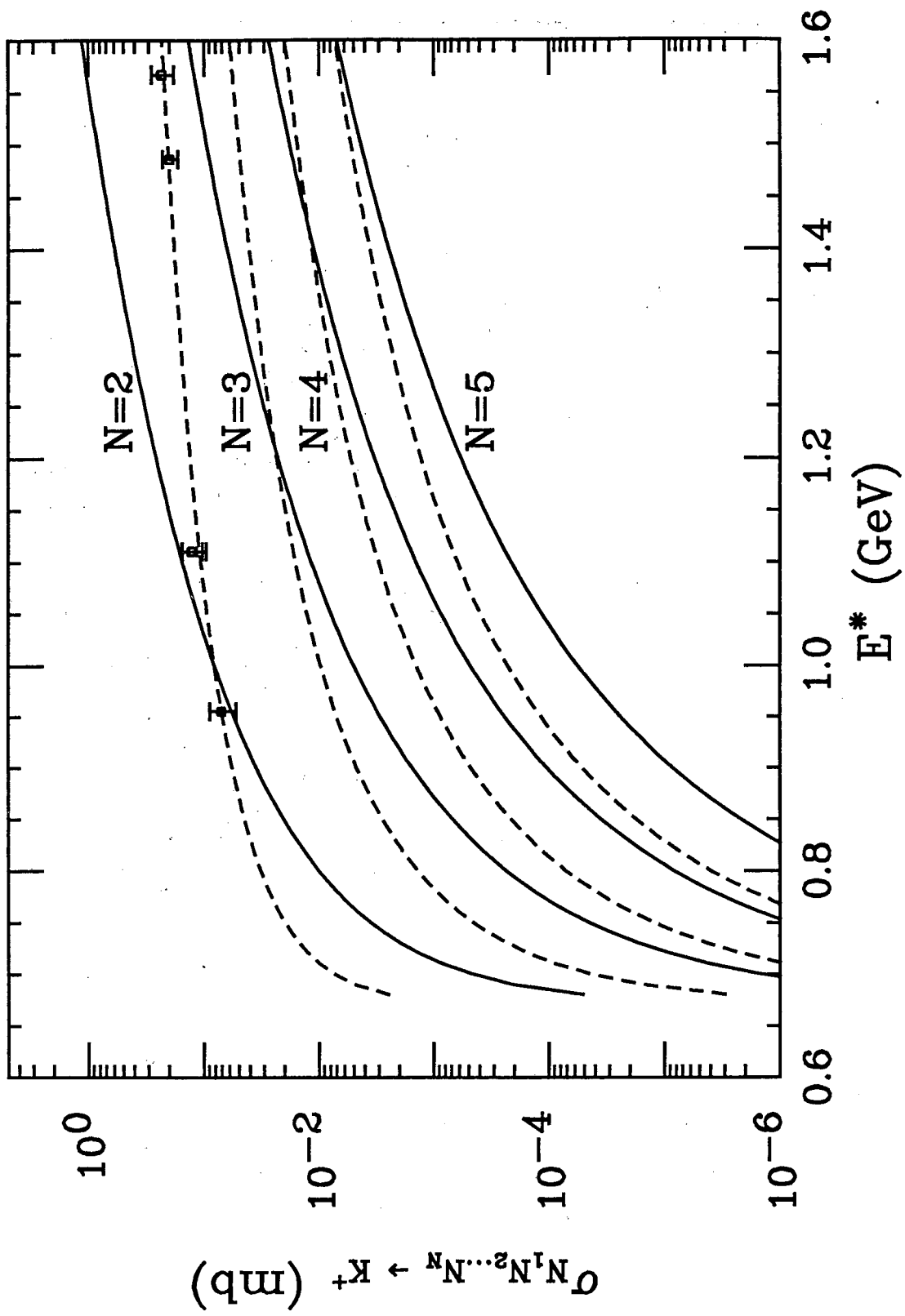


Figure 11

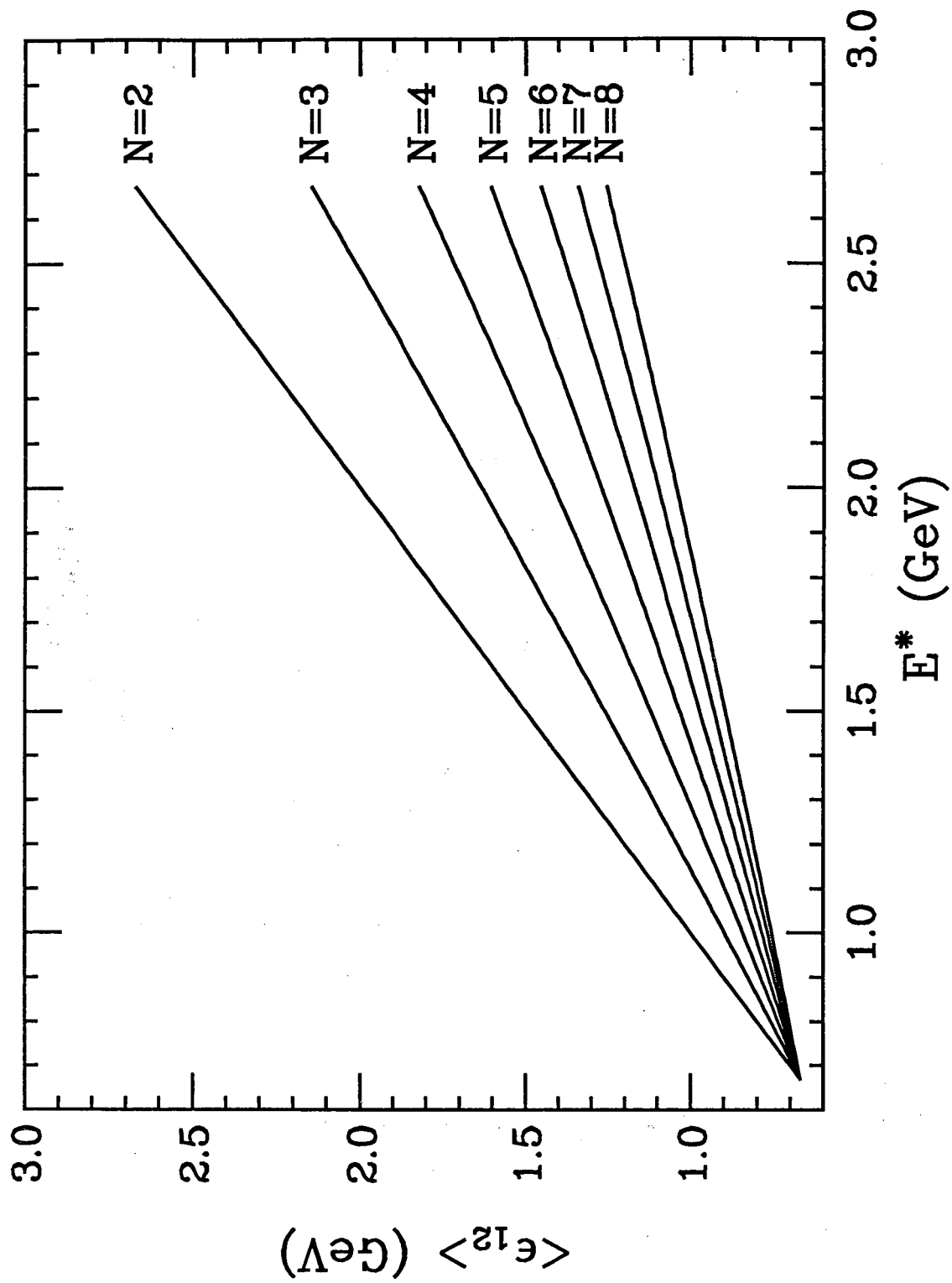


Figure 12

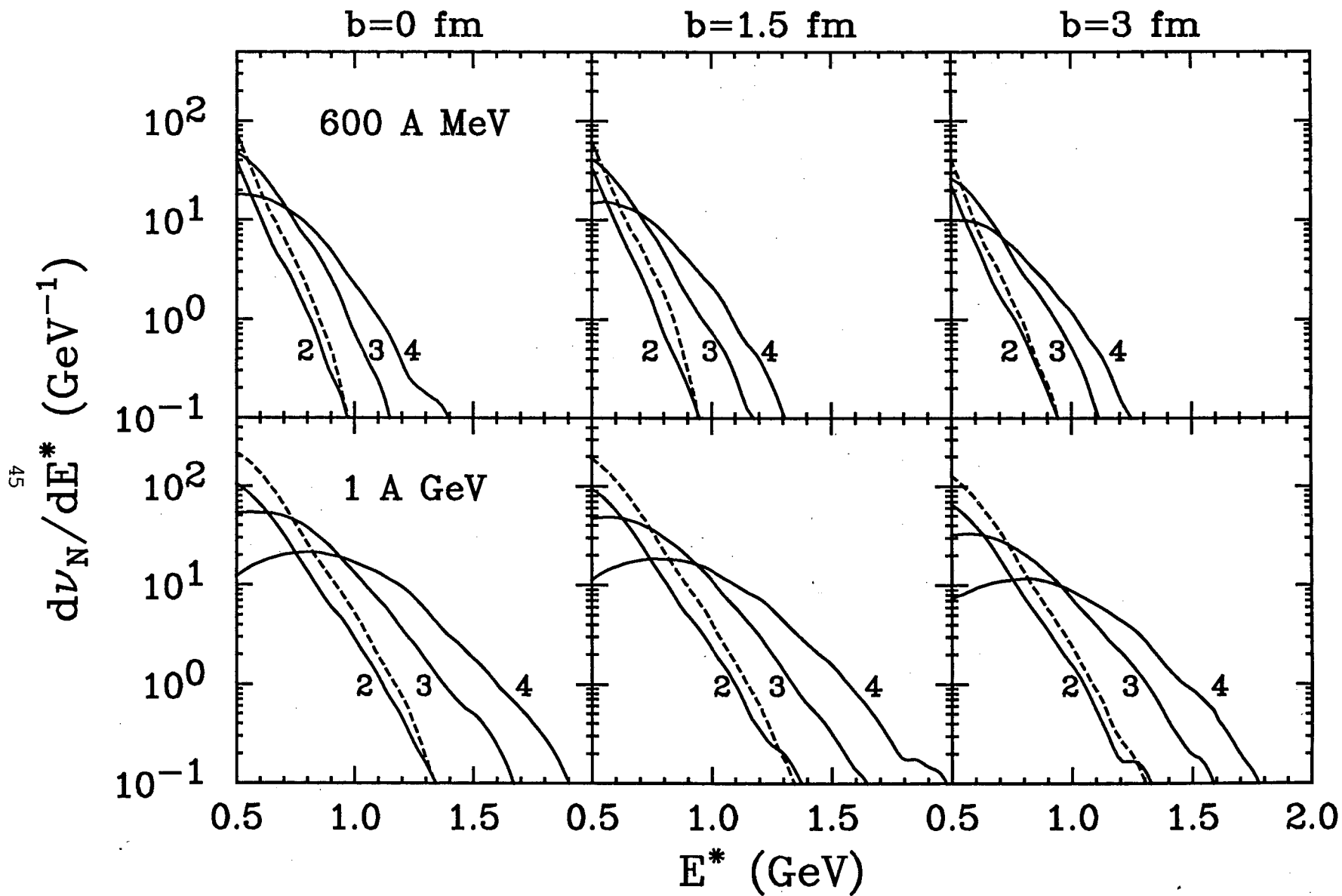


Figure 13

$^{40}\text{Ca} + ^{40}\text{Ca}$

$b=0$

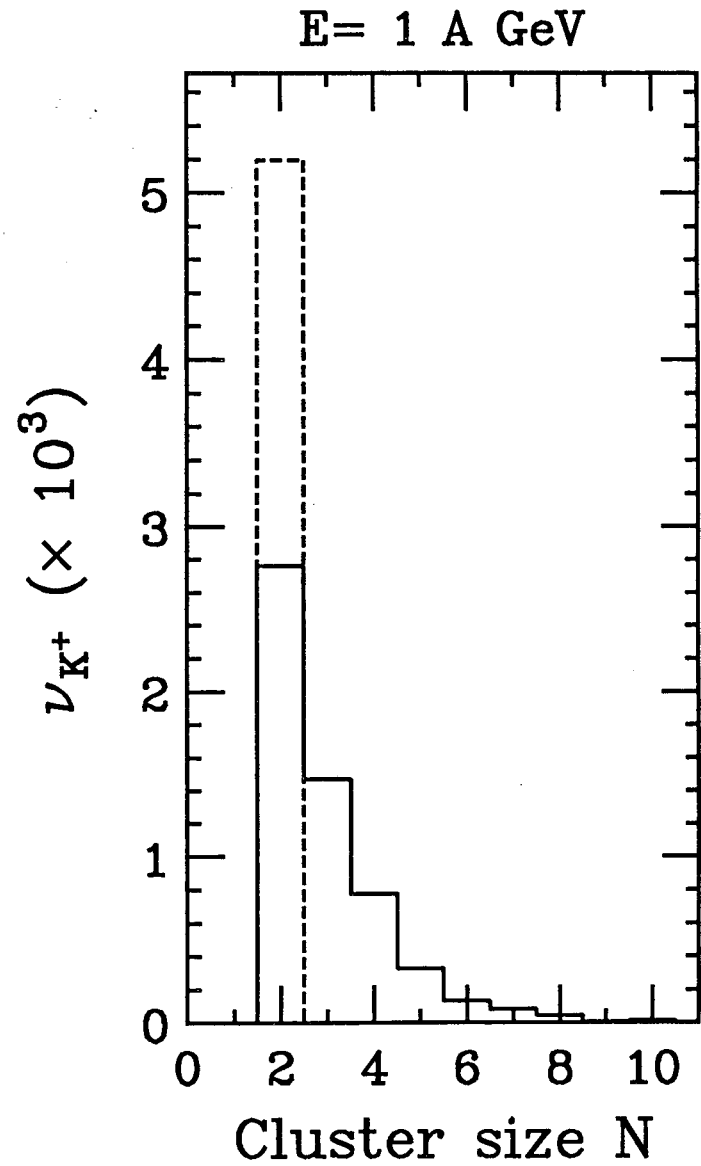
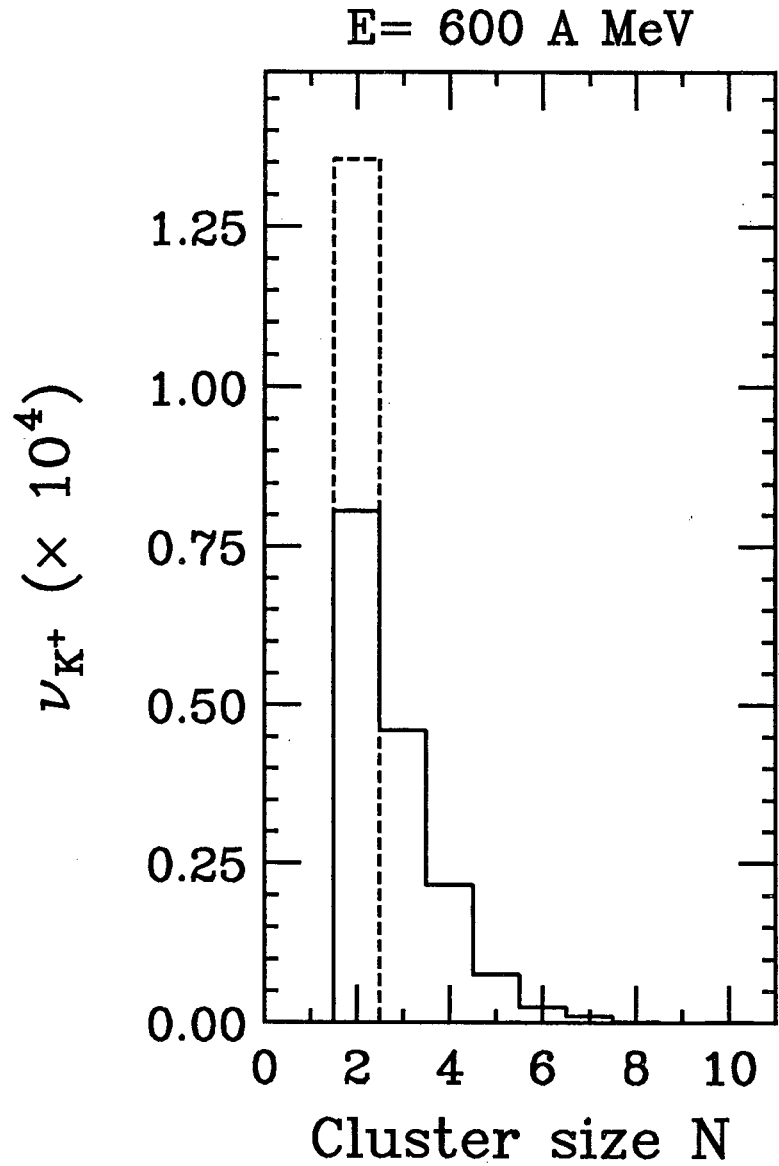
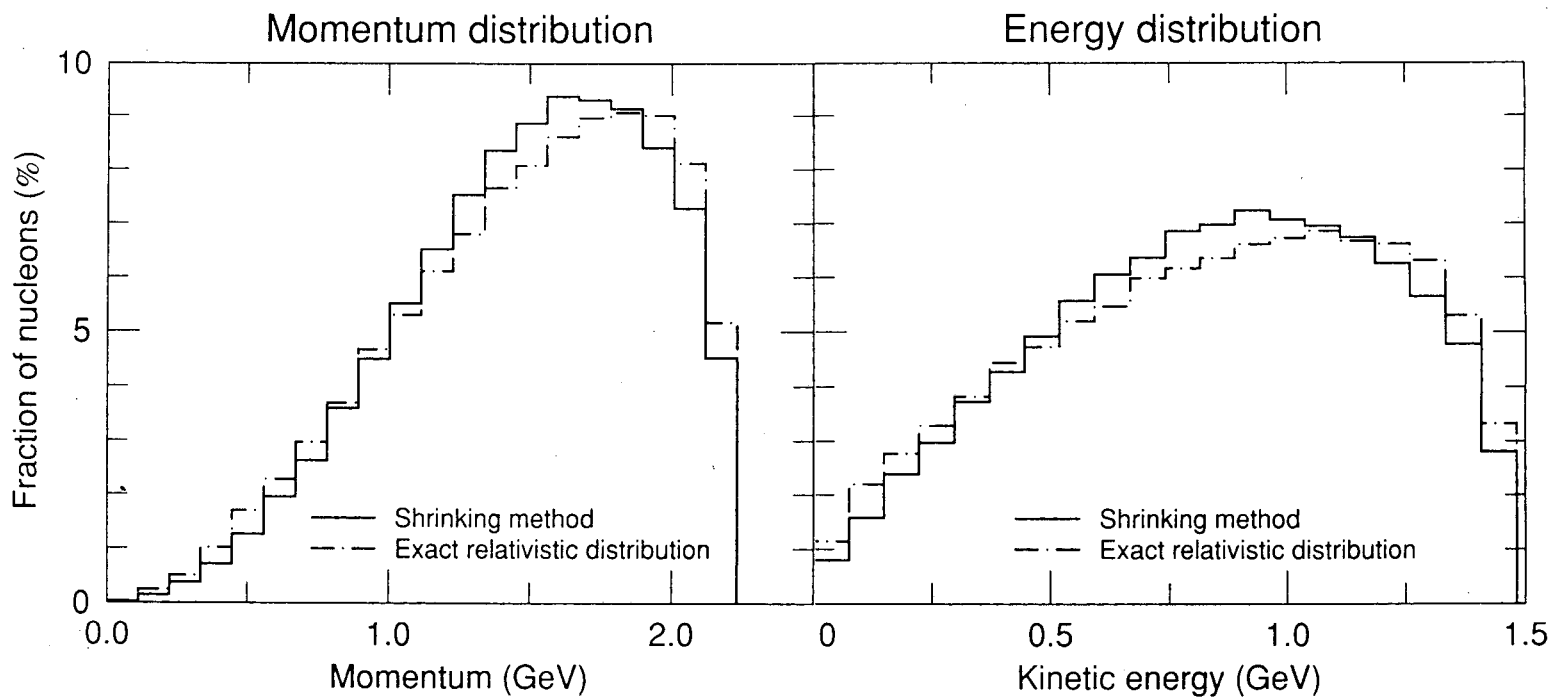


Figure 14



XBL 917-1459

Figure 15

LAWRENCE BERKELEY LABORATORY
UNIVERSITY OF CALIFORNIA
INFORMATION RESOURCES DEPARTMENT
BERKELEY, CALIFORNIA 94720